Journal of Geosciences, 52 (2007), 73–112 DOI: 10.3190/jgeosci.010

Original paper

Hyperpotassic granulites from the Blanský les Massif (Moldanubian Zone, Bohemian Massif) revisited

Vojtěch JANOUŠEK[1, 2]*, Erwin KRENN[3], Fritz FINGER[3], Jitka MÍKOVÁ[1], Jiří FRÝDA[1]

[1]*Czech Geological Survey, Klárov 3, 118 21 Prague 1, Czech Republic; janousek@cgu.cz*
[2]*Institute of Petrology and Structural Geology, Charles University, Albertov 6, 128 43 Prague 2, Czech Republic*
[3]*Division of Mineralogy and Material Science, University of Salzburg, Hellbrunnerstraße 34, A-5020 Salzburg, Austria*
[*]*Corresponding author*

In the Blanský les granulite Massif (Moldanubian Unit, South Bohemia), built mainly by felsic calc-alkaline HP–HT garnet ± kyanite granulite, occur rare small bodies of hyperpotassic granulite with garnet (Plešovice type) or pyroxene (Lhotka type).

The *Plešovice type* is dominated by slightly perthitic K-feldspar and almandine–pyrope rich garnet, the latter variously retrogressed to biotite ± plagioclase. The other conspicuous euhedral crystals are apatite and zircon. In the rock occur also Zr–Nb-rich rutile and much rarer primary monazite; originally LREE-rich apatites decompose into small Th-poor, MREE-rich monazite grains.

The *Lhotka type* granulites contain pyroxene, often altered to actinolite, instead of garnet. The predominant perthitic K-feldspar encloses a small amount of unmixed celsian. Typical are large euhedral crystals of apatite with small unmixed monazite grains; primary monazite is rare. Noteworthy is the occurrence of secondary Ti phases with high REE, Y and Zr, formed at the expense of the primary pyroxene.

The studied granulite types are highly potassic (K_2O > 7 %, up to *c.* 14 %, K_2O/Na_2O = 3.1–9.2 wt. %), silica-poor (SiO_2 < 65 %), with low contents of most major- and minor-element oxides, apart from K and P. Characteristic are high concentrations of Cs, Rb, Ba and U at variable enrichments in Zr and Hf. Whole-rock contents some HFSE (Ti, Nb and Ta) are extremely low. The REE patterns show marked negative Eu anomalies and variable LREE enrichments increasing with rising silica due to a conspicuous drop in HREE. The Sr–Nd isotopic ratios document the derivation from mature crustal sources (ε_{Nd}^{337} ~ -5.5; $^{87}Sr/^{86}Sr_{337}$ = 0.7272 and 0.7279 for the Plešovice and $^{87}Sr/^{86}Sr_{337}$ = 0.7109 for the Lhotka types). Apatite saturation temperatures are high (~1070 °C), close to the previously estimated conditions of (re)crystallization for both calc-alkaline and hyperpotassic granulites. The zircon saturation temperatures tend to be more variable, some exceeding 1000 °C but many unrealistically low, reflecting effects of disequilibrium melting, heterogeneous distribution of accumulated crystals in the magma and/or sampling bias.

The hyperpotassic granulites are interpreted as Viséan igneous rocks. The parental magma could have originated by low degrees of HP–HT, non-eutectic partial melting. The low-scale melt was most likely expelled close to the HP–HT metamorphic peak or at early stages of decompression from common Moldanubian calc-alkaline granulites. This genetic link is documented by the presumed P-T conditions, similar age and complementary geochemical and Sr–Nd isotopic signatures. Subsequently the magma could have developed by garnet, apatite and zircon dominated fractional crystallization, with or without some crystal accumulation.

Keywords: granulites, alkali feldspar syenites, high-pressure melting, geochemistry, Moldanubian Zone, Bohemian Massif
Received: 29 January 2007; accepted 6 June 2007; handling editor: M. Novák

1. Introduction

Felsic (granitic) calc-alkaline garnet ± kyanite-bearing high-pressure and high-temperature (HP–HT) granulites form an important constituent of the high-grade Moldanubian Zone, interpreted as an orogenic root of the European Variscan orogen in Central Europe (e.g., Fiala et al. 1987a; Vrána and Šrámek 1999; O'Brien and Rötzler 2003; O'Brien 2006; Kotková this volume). Regardless the attention the classic occurrences of these granulites in South Bohemia, Western Moravia and Lower Austria (Fig. 1a–b) have attracted, their genesis still remains open to debate. They have been interpreted as metamorphosed older, mostly felsic igneous or volcanosedimentary rocks (e.g., Fiala et al. 1987a; Vellmer 1992). In this case, some amount of trapped high-pressure melt was likely to have been present, even though its proportion is not well constrained yet: less than 10–15 vol. % (Roberts and Finger 1997; Janoušek et al. 2004) or up to 20–30 vol. % (Tropper et al. 2005). Alternatively, some of the felsic granulites were interpreted as separated Viséan (~340 Ma) dry, HP–HT (P > 15 kbar, T > 1000 °C) partial melts of metasedimentary lithologies (Vrána 1989; Jakeš 1997; Kotková and Harley 1999) or of granitoids/acid volcanic rocks (Vrána 1989). As a third, and so far little tested model, Viséan HP metamorphism (P up to 18 kbar,

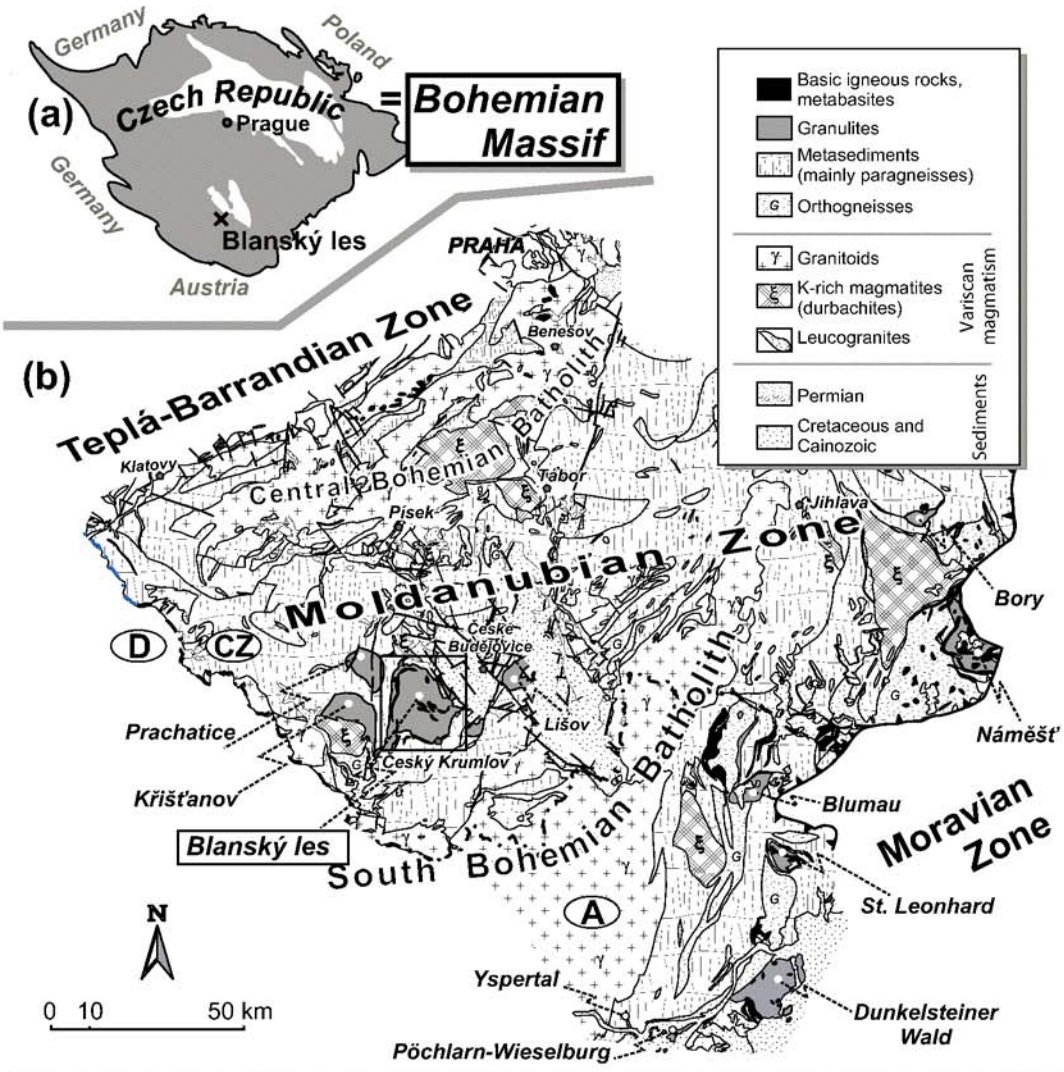

Fig. 1 a – Location of the Blanský les granulite body within the Bohemian Massif. **b** – Geological sketch of the Moldanubian Zone in Southern Bohemia and Lower Austria (modified from the Czech Geological Survey map 1:500 000). **c** – Schematic map of the Blanský les granulite Massif (after Kodym et al. 1978) with location of the localities mentioned in the text.

T ~ 800 °C) of pre-existing mid-crustal (P = 8–10 kbar) hypersolvus granites has been invoked by Štípská and Powell (2005).

More than fifteen years ago (Vrána 1989), a special type of rare highly potassic granulites (referred to as hyperpotassic granulites here) has been discovered in the Blanský les granulite Massif (South Bohemia) that may shed some light onto this long standing controversy. Only several small bodies of these rocks have been recorded to date, enclosed within overwhelming volumes of mainly felsic calc-alkaline, HP (Grt ± Ky) granulites. Striking is their unusual modal composition dominated by alkali feldspar, prevailing over garnet, apatite and zircon, all in relatively large crystals. Even though volumetrically subordinate, these rocks provided invaluable handle on the timing of the Variscan HP metamorphism in the Moldanubian Zone (Aftalion et al. 1989). Recently they have triggered renewed interest due to an analytical effort to establish their unusually big zircons as an international standard for Hf isotopic determinations and U–Pb LA ICP-MS dating (Sláma et al. 2006).

In his pioneering work, Vrána (1989) dealt with the petrography and whole-rock geochemistry of the garnet-bearing hyperpotassic granulites from the Plešovice quarry. He concluded that these rocks could be products of high-pressure, non-eutectic anatexis of a metasedimentary or metaigneous protolith, further modified by HP fractional crystallization and decompression. Some ten years later, the same author added a brief description of a subordinate, pyroxene-bearing subtype from Lhotka (Vrána 1998).

However, little has been done to characterise the mineral, whole-rock and isotopic geochemistry of the unusual hyperpotassic granulites from the Blanský les granulite Massif ever since. The present paper attempts to fill this gap, in order to further constrain the petrogenesis of these enigmatic rocks. Moreover, it addresses the issue of the mechanism and importance of HP–HT melting in the history of large felsic calc-alkaline granulite bodies scattered throughout much of the Moldanubian Zone.

2. Geological setting

2.1. Moldanubian Zone

In the southern part of the Bohemian Massif, shared by the Czech Republic and Austria, the Moldanubian Zone consists of several crustal segments with contrasting age and complex polyphase deformational histories, intruded by numerous large, mostly Carboniferous granitic plutons (Fuchs 1976; Dallmeyer et al. 1995; Finger et al. 1997) (Fig. 1). Apart from tectonically displaced segments of the Early Proterozoic basement (e.g., ~2.1 Ga Světlík orthogneiss in S Bohemia: Wendt et al. 1993; ~1.38 Ga Dobra orthogneiss in Lower Austria: Gebauer and Friedl 1994), the allochthonous Moldanubian sequence has been subdivided into a structurally lower and mainly metasedimentary, amphibolite-facies Drosendorf and above this, a higher grade Gföhl assemblages (Fuchs and Matura 1976; Matte et al. 1990; Fiala et al. 1995; Franke 2000).

2.1.1. Drosendorf Assemblage

The lower part of the Drosendorf Assemblage consists of the Monotonous Unit made up mainly of cordierite–biotite–sillimanite paragneisses, which are partly migmatitic and contain intercalations of orthogneisses and minor amphibolites. The upper part, termed Varied Unit, contains paragneisses, orthogneisses, amphibolites, carbonate rocks, calc-silicate gneisses, quartzites and graphite schists (e.g., Fiala et al. 1995).

2.1.2. Gföhl Assemblage

The Gföhl Assemblage is built by a heterogeneous blend of high-pressure crustal and upper mantle rocks, assembled and exhumed during the Variscan orogeny (Fiala et al. 1995; O'Brien and Rötzler 2003). While the lower parts of the unit in Austria and the Náměšť Massif in Moravia include mainly anatectic orthogneisses (Gföhl Gneiss), the higher are dominated by granulites, associated with lesser bodies of garnet/spinel peridotites, garnet pyroxenites and eclogites (e.g., Fuchs and Matura 1976; Urban 1992; Fiala et al. 1995; O'Brien and Rötzler 2003; Medaris et al. 2005, 2006). The whole assemblage has been long interpreted as remnants of a large-scale Gföhl nappe (Tollmann 1982; Franke 1989), although more recently a tectonic exhumation along steep structures has been considered possible, if not more likely (Vrána and Šrámek 1999; Franěk et al. 2006; Racek et al. 2006; Finger et al. this volume).

Among the granulites, there are subordinate mafic–intermediate pyroxene-bearing types (primary HT mineralogy: hypersolvus feldspar converted to antiperthite + quartz + plagioclase + orthopyroxene + biotite ± garnet ± clinopyroxene ± K-feldspar), and scarce sedimentary-derived granulites (Fiala et al. 1987b). However, the felsic granulites (SiO_2 >70 %) are by far the most abundant, accounting for > 75–80 % by volume (Fiala et al. 1987a; Vellmer 1992). They are characterized by the relics of the massive texture with the original HP assemblage hypersolvus feldspar (now mesoperthite) + quartz + garnet ± kyanite; zircon, apatite, ilmenite, rutile ± monazite are the common accessories (Fiala et al. 1987a, b; Carswell and O'Brien 1993; O'Brien and Rötzler 2003; Janoušek et al. 2004; O'Brien 2006).

2.1.3. Blanský les granulite Massif

The Blanský les granulite Massif (BLGM) located SW of České Budějovice, is an oval-shaped body (*c.* 24 ×14 km), surrounded by amphibolite-facies metamorphic rocks of both Monotonous and Varied units (e.g., O'Brien and Carswell 1993; Fiala et al. 1995) (Fig. 1c).

The main rock type in the BLGM is a calc-alkaline, high-pressure felsic (SiO_2 >70 %), garnet ± kyanite granulite, strongly prevailing over mafic (mainly pyroxene-bearing) granulite, garnet peridotite and eclogite (Fediuková 1978; Kodym et al. 1978; Vrána 1979; Slabý 1983; Strejček 1986; Fiala et al. 1987a, b; Vrána 1992). Common are intercalations of more basic garnet–biotite granulitic gneiss, sometimes with kyanite and sillimanite, some of which might be of metasedimentary origin. The peculiar hyperpotassic, zircon-rich (K_2O up to ~14 %, Zr up to 5000 ppm), garnet-bearing granulites (Vrána 1989) are mainly found in the Plešovice quarry.

Much of the information on the variability of the BLGM comes from the *c.* 1500 m deep borehole H-1 drilled at Holubov, 8 km N of Český Krumlov, in 1965. It penetrated mainly granulitic rocks, again with leucogranulites prevailing over the more mafic types. The rest was accounted for by several tectonic slices of ultrabasic rocks and the whole assemblage was cut by infrequent dykes of Variscan aplites–pegmatites (Kodym et al. 1978; Fediuková 1978; Janoušek et al. 2004).

The structural geology of the BLGM and its emplacement mechanism have been dealt with by Kodym (1972); Vrána (1979); Rajlich et al. (1986); Vrána and Šrámek (1999); Svojtka et al. (2002) and newly Franěk et al. (2006). Summary of the available P-T estimates and PTt development can be found in Pin and Vielzeuf (1983); Owen and Dostal (1996); Vrána and Šrámek (1999); Kröner et al. (2000); Svojtka et al. (2002); Štípská and Powell (2005) as well as Franěk et al. (2006).

2.1.4. The age of the Variscan high-pressure metamorphism in the South Bohemian granulite massifs

Calc-alkaline granulites Based on an extensive database of conventional zircon and monazite U–Pb ages, the granulite-facies metamorphism in the Moldanubian Zone of South Bohemia is thought to have taken place at Viséan times, at *c.* 340 Ma ago (van Breemen et al. 1982; Wendt et al. 1994). Arguably the best chronological constraint for the HP event is the mean of SHRIMP ages (339.8 ± 2.6 Ma) reported for multifaceted zircon grains from calc-alkaline South Bohemian granulites (Kröner et al. 2000).

On the other hand Svojtka et al. (2002) placed, based on Sm–Nd ages for garnet cores with prograde zoning, the HP-HT metamorphic peak *c.* 10–15 Ma earlier. However the previous Sm–Nd and U–Pb Grt–WR dating of the Moldanubian granulites yielded a broad spectrum of (mostly spurious) ages scattered between the likely protolith intrusion and HP metamorphism (Janoušek et al. 1996; Chen et al. 1998). As shown by Romer and Rötzler (2001), the Sm–Nd garnet ages do not have to date the HP-HT metamorphic peak at all. Instead, they may reflect imperfect re-equilibration of garnet with the whole-rock Sm–Nd system caused by distinct reaction histories of individual dated garnets, replacing different primary phases at a range of prograde P-T conditions. This would be particularly likely if the burial was rapid and significant amounts of fluid were absent (Villa 1998).

A summary of the available geochronological data (including the protolith ages) for Moldanubian granulites has been given by Kröner et al. (2000), Schulmann et al. (2005) and Janoušek and Holub (2007).

Hyperpotassic granulites Somewhat younger appears the nearly concordant U–Pb zircon age of 338 ± 1 Ma from hyperpotassic granulites of the BLGM with a badly defined upper intercept of 600 ± 200 Ma (Aftalion et al. 1989). Sláma et al. (2006) revisited the locality and analysed large (up to several mm), euhedral and nearly unzoned zircons in this rock as a newly established international geochemical standard *PL*. Thanks to their analytical efforts the Plešovice hyperpotassic granulites became probably the most dated granulite body worldwide. The obtained ages are well comparable both mutually as well as with the results of Aftalion et al. (1989): 337.1 ± 0.7 Ma (TIMS, University of Geneva), 338 ± 1 Ma (LA ICP-MS, University of Bergen), 336 ± 1 Ma (LA ICP-MS, Memorial University of New Foundland), and 335 ± 1 Ma (LA ICP-MS, Natural History Museum, London). Weighted average of these four new determinations is 336.6 ± 0.6 Ma.

Significant for interpretation of the U–Pb geochronological data from the calc-alkaline (Kröner et al. 2000) and hyperpotassic (Aftalion et al. 1989) granulites is the fact the dated zircons were enclosed in hypersolvus feldspar and garnet, the HT and HP phases. Thus it is hard to envisage that the timing of the HP metamorphic peak and crystallization of hyperpotassic granulites would have been very different from *c.* 340 Ma and *c.* 337 Ma, respectively.

3. Analytical techniques

3.1. Cathodoluminescence

The optical cathodoluminescence (CL) observations were made using a CITL Technosyn 8200 Mk 4 at University of Glasgow. Typical operating conditions were 26 kV,

with a gun current of 210 μA, and a vacuum of approximately 1.2 mbar. Images were recorded on a Nikon DN100 digital camera.

3.2. Mineral chemistry

Analyses were carried out on JEOL JX 8600 electron microprobe analyser (EMPA) at Salzburg University equipped with four wave-dispersive spectrometers. All analyses were performed at an acceleration voltage of 15 kV but with different beam currents and spot sizes chosen according to mineral type and grain/domain size (zoning type). Thus 100 nA and a spot size of 1 and 5 μm were employed for analysing pyroxene, titanite, rutile and monazite. For apatite, feldspars and micas the beam spot was defocused to 10–15 μm using beam currents of 25 nA for feldspars and 25–100 nA for apatites. Table 1 gives details of the analytical settings for 100 nA, the standards used, the counting times and detection limits for individual elements. The errors resulting from counting statistics at 100 nA were *c.* 0.006–0.04 (1σ; except for F) at concentrations up to 1 wt. %; at higher concentrations the statistical error was better than 0.15 wt. % (1σ). Final element concentrations were obtained using ZAF-correction. Minor element interferences have been checked routinely and corrected for by measuring the corresponding standards. Due to the profound Ti–Ba or Ba–Ce interferences, Ba and Ce could not be precisely determined in Ti- or Ba-rich grains, respectively.

The mineral analyses were recalculated using the R package *GCDkit-Mineral* (Janoušek et al. 2006c).

Tab. 1 Analytical conditions, electron microprobe measurements

100 nA 15 kV element	Line	Crystal	Standard	Counting time on peak/ background (s)	Detection limit 3 sigma (wt. %)
Mg	Kα	TAP	MgO	10 (2×5)	0.02
Al	Kα	TAP	$Y_3Al_5O_{12}$	10 (2×5)	0.02
Si	Kα	TAP	quartz	10 (2×5)	0.02
P	Kα	PET	monazite	10 (2×5)	0.08
S	Kα	PET	PbS	10 (2×5)	0.03
Ca	Kα	PET	wollastonite	10 (2×5)	0.08
Ti	Kα	PET	TiO_2	10 (2×5)	0.04
Cr	Kα	LIF	chromite	10 (2×5)	0.04
Mn	Kα	LIF	MnO	10 (2×5)	0.04
Fe	Kα	LIF	metallic Fe	10 (2×5)	0.04
Sr	Lα	LIF	glass	20 (2×10)	0.04
Ba	Lα	LIF	glass	30 (2×15)	0.07
Y	Lα	PET	$Y_3Al_5O_{12}$	10 (2×5)	0.06
La	Lα	PET	monazite	20 (2×10)	0.06
Ce	Lα	PET	monazite	20 (2×10)	0.06
Pr	Lβ	LIF	monazite	50 (2×25)	0.10
Nd	Lβ	LIF	monazite	30 (2×15)	0.08
Sm	Lβ	LIF	glass	40 (2×20)	0.08
Gd	Lβ	LIF	glass	50 (2×25)	0.10
Dy	Lα	LIF	glass	50 (2×25)	0.10
Er	Lβ	LIF	glass	50 (2×25)	0.11
Yb	Lα	LIF	YbF_3	50 (2×25)	0.07
Zr	Lα	PET	zircon	20 (2×10)	0.05
Hf	Mα	PET	zircon	40 (2×20)	0.08
Pb	Mα	PET	PbS	30 (2×15)	0.07
Th	Mα	PET	metallic Th	20 (2×10)	0.08
U	Mα	PET	metallic U	20 (2×10)	0.08

3.3. Whole-rock geochemistry

Most of the major-element whole-rock analyses were performed by wet chemistry in the laboratories of the Czech Geological Survey, Prague–Barrandov. The relative 2σ uncertainties were better than 1 % (SiO_2), 2 % (FeO), 5 % (Al_2O_3, K_2O, Na_2O) 7 % (TiO_2, MnO, CaO), 10 % (Fe_2O_3) and 15 % (but mainly < 6 %, MgO).

A few of the major-element analyses and most trace elements were determined by XRF (Bruker AXS) at the Division of Mineralogy and Material Science, University of Salzburg on lithium tetraborate glass beads and pressed pellets, respectively. The tube conditions (max: 4 kW and 60 kV) and the counting time was optimised automatically in order to obtain a detection limit of *c.* 1 ppm. Typical errors from the counting statistics were ± 1 ppm at low concentrations (< 10 ppm) and better than ± 5 % (relative) for the rest.

In addition, several samples were analysed in the Acme Analytical Laboratories, Vancouver, Canada. The majority of the trace elements in this case were determined by $LiBO_2/Li_2B_4O_7$ fusion and ICP-MS/ES, except for precious and base metals analysed by aqua regia digestion followed by ICP-MS.

3.4. Radiogenic isotopes

For the isotopic study, samples were dissolved using a combined HF–HCl–HNO_3 attack. Strontium was isolated by exchange chromatography techniques on PP columns with Sr.spec Eichrom resin and bulk REE were isolated on PP columns filled with TRU.spec Eichrom resin (Pin et al. 1994). The Nd was further separated on PP columns with Ln.spec Eichrom resin (Pin and Zalduegui 1997).

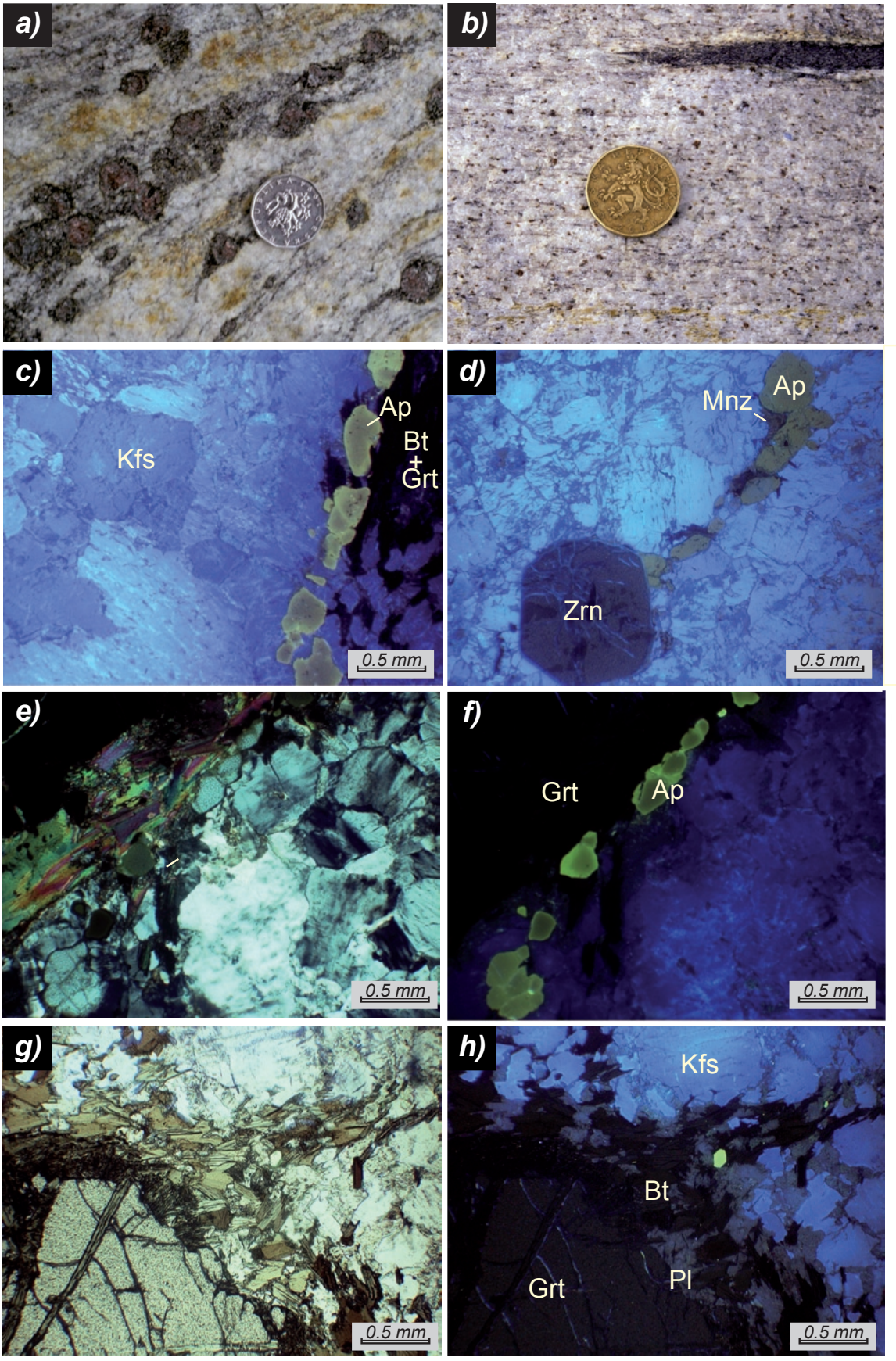
a)
b)
c)
Kfs
Ap
Bt
+
Grt
0.5 mm
d)
Mnz
Ap
Zrn
0.5 mm
e)
0.5 mm
f)
Grt
Ap
0.5 mm
g)
0.5 mm
h)
Kfs
Bt
Grt
Pl
0.5 mm

Tab. 2 Selected feldspar analyses recalculated on the basis of 8 O

	Garnet granulite UK3 (Plešovice type)				*Garnet granulite UK1 (Plešovice type)*				*Pyroxene granulite UK5 (Lhotka type)*			
Mineral	Kfs	Kfs	Pl	Pl	Kfs	Pl	Pl	Pl	Kfs	Kfs	Ab	Ba Fsp
BSE fig	Fig. 3a/A	Fig. 3a/C			Fig. 3c/13	Fig. 3b/22	Fig. 3d/1	Fig. 3d/3	Fig. 6b/1	Fig. 6b/2	Fig. 6a/3	Fig. 6a/4
Desc	bright domain in Kfs	bright domain in Kfs	exolution Ab rich	large Pl with An-rich core	Kfs with Pl exolutions	Pl-exolution, Ab rich	large Pl with An-rich core	large Pl with Ab-rich rim	bright domain	dark domain	perthite	spotty exsolution
SiO_2	64.07	64.15	69.89	64.10	64.42	67.60	65.35	68.99	64.33	63.93	67.37	32.24
Al_2O_3	18.77	18.25	20.06	23.60	18.54	21.58	20.70	20.00	18.10	17.95	18.88	25.48
P_2O_5	0.05	0.05	0.01	0.01	0.05	0.08	0.00	0.07	b.d.	b.d.	b.d.	b.d.
CaO	0.05	0.01	0.16	4.47	0.02	0.13	3.12	0.20	b.d.	b.d.	0.06	0.07
FeO	0.06	0.00	0.07	0.02	0.00	0.00	0.00	0.00	0.15	0.17	0.06	0.53
MgO	b.d.	b.d.	b.d.	b.d.	b.d.	b.d.	b.d.	b.d.	b.d.	b.d.	b.d.	0.32
MnO	b.d.	b.d.	b.d.	b.d.	b.d.	b.d.	b.d.	b.d.	b.d.	b.d.	b.d.	b.d.
TiO_2	b.d.	b.d.	b.d.	b.d.	b.d.	b.d.	b.d.	b.d.	b.d.	b.d.	b.d.	b.d.
Cr_2O_3	b.d.	b.d.	b.d.	b.d.	b.d.	b.d.	b.d.	b.d.	b.d.	b.d.	b.d.	b.d.
K_2O	15.25	16.26	0.15	0.42	14.69	0.15	0.10	0.13	15.45	16.79	0.11	0.87
Na_2O	0.93	0.34	11.71	9.29	1.42	11.38	9.98	11.73	1.30	0.49	11.98	0.08
BaO	0.18	0.17	0.01	0.00	0.26	0.07	0.01	0.00	0.53	0.60	0.00	[a]34.60
SrO	b.d.	b.d.	b.d.	b.d.	b.d.	b.d.	b.d.	b.d.	b.d.	b.d.	b.d.	b.d.
Total	99.34	99.23	102.06	101.92	99.39	101.00	99.27	101.14	99.85	99.92	98.47	[a]94.20
Si (apfu)	2.976	2.991	2.988	2.783	2.984	2.925	2.896	2.978	2.999	2.998	3.003	2.044
Al	1.027	1.003	1.011	1.208	1.012	1.100	1.081	1.018	0.994	0.992	0.992	1.904
Fe	0.002	0.000	0.002	0.001	0.000	0.000	0.000	0.000	0.006	0.007	–	0.028
Mg	–	–	–	–	–	–	–	–	–	–	–	0.030
K	0.904	0.967	0.008	0.023	0.868	0.008	0.006	0.007	0.873	0.955	0.006	0.067
Na	0.083	0.031	0.970	0.782	0.127	0.954	0.857	0.982	0.117	0.044	0.984	0.009
Ba	0.003	0.003	0.000	0.000	0.005	0.001	0.000	0.000	0.010	0.011	0.000	0.859
Ca	0.002	0.000	0.007	0.208	0.001	0.006	0.148	0.009	–	–	–	–

[a] probably too low due to the low Ba concentration in the standard (~10 wt.% BaO)

Isotopic analyses were performed on Finnigan MAT 262 thermal ionization mass spectrometer in dynamic mode using a double Re filament assembly (CGS). The $^{143}Nd/^{144}Nd$ ratios were corrected for mass fractionation to $^{146}Nd/^{144}Nd = 0.7219$, $^{87}Sr/^{86}Sr$ ratios assuming $^{86}Sr/^{88}Sr = 0.1194$. External reproducibility is given by results of repeated analyses of the La Jolla ($^{143}Nd/^{144}Nd = 0.511852 \pm 14$ (2σ), n = 23) and NBS 987 ($^{87}Sr/^{86}Sr = 0.710247 \pm 26$ (2σ), n = 25) isotopic standards. The Rb, Sr, Sm and Nd concentrations were obtained by ICP-MS in Acme Analytical Laboratories, Canada.

The decay constants applied to age-correct the isotopic ratios are from Steiger and Jäger (1977) (Sr) and Lugmair and Marti (1978) (Nd). The ε^{i}_{Nd} values and single-stage CHUR Nd model ages were obtained using Bulk Earth parameters of Jacobsen and Wasserburg (1980), the two-stage Depleted Mantle Nd model ages (T^{DM}_{Nd}) were calculated after Liew and Hofmann (1988).

⇐

Fig. 2 Field photographs from the working quarry Plešovice (a, b), photomicrographs (e, g) and cathodoluminescence images of the hyperpotassic granulite UK1 (c, d, f, h). **a)** Hyperpotassic granulite with little retrogressed garnet crystals, right part of the quarry (the diameter of the coin is 21 mm). **b)** Ky–Grt felsic granulite, highermost quarry bench, central part (the coin is 26 mm across). **c)** CL photomicrograph, on which are clearly discernible two generations of K-feldspar (various shades of blue), one of them strongly perthitic. The yellow–orange apatites in a linear cluster are distinctly zoned, with brighter rims. Non-luminescent minerals are biotite and garnet. **d)** Large euhedral zircon crystal (low-luminescent) in a K-feldspar matrix. The string of apatite crystals is intimately associated with interstitial, brownish (CL) secondary monazite. **e), f)** Another cluster of distinctly zoned apatite crystals at a boundary between non-luminescent garnet and bluish K-feldspar. **g), h)** Relict garnet, breaking down to biotite and a fine aggregate of plagioclase with quartz. Two bright yellow euhedral crystals (CL) of apatite are present in the K-feldspar matrix.

4. Petrology and mineral chemistry of the hyperpotassic granulites

4.1. Garnet-bearing hyperpotassic granulites (Plešovice type)

Vrána (1989) described hyperpotassic garnet-bearing granulites from the active quarry in Plešovice, *c.* 15 km SE of České Budějovice (close to the SE margin of the Blanský les granulite Massif: Fig. 1c). The light grey to ochre orange rocks (Fig. 2a) occur as foliated layers several me-

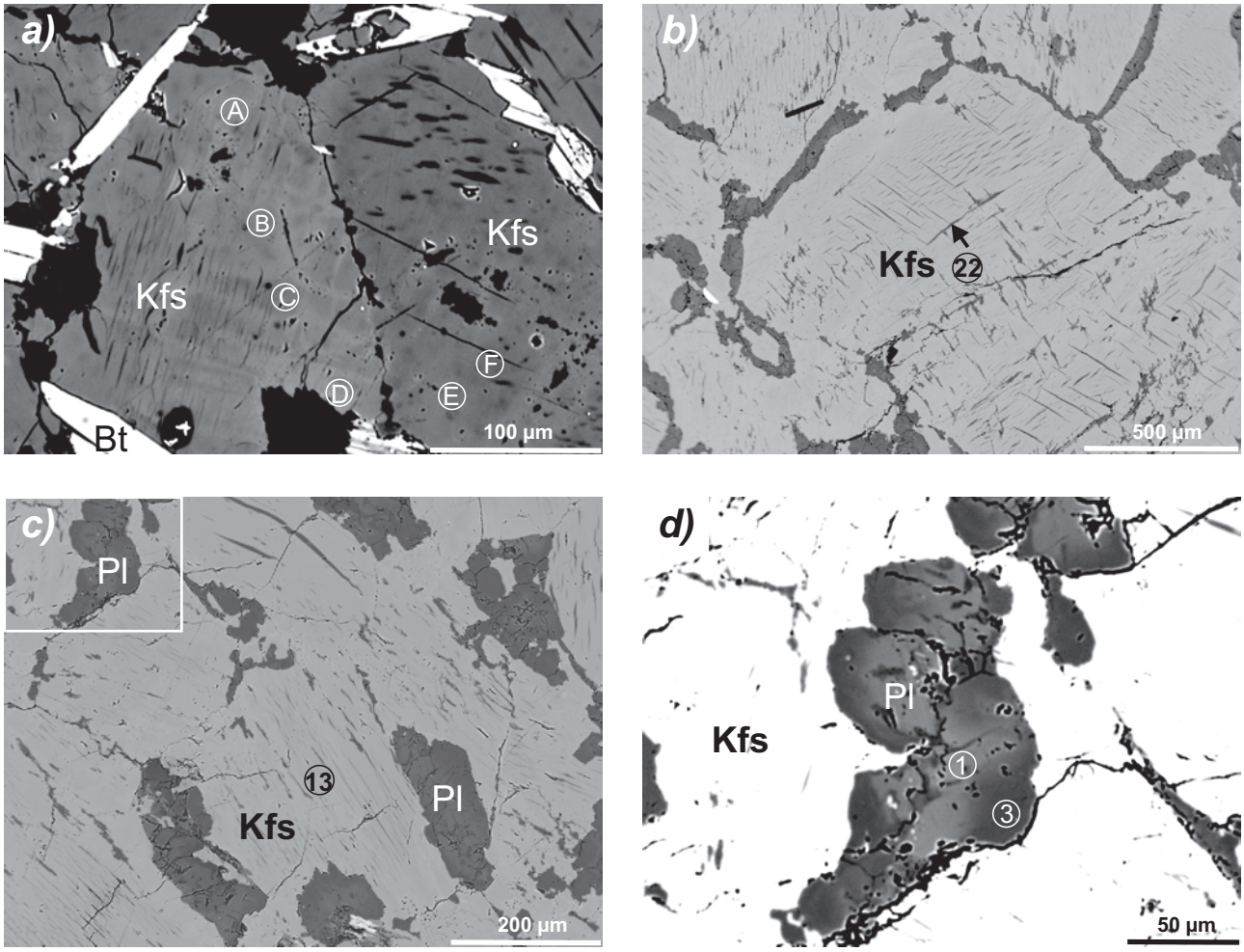

Fig. 3 Backscattered electron (BSE) images of alkali feldspars from the garnet-bearing hyperpotassic granulites. **a)** Patchy zoning in K-feldspar from sample UK3. Selected analyses are given in the Tab. 2. **b)** Two types of exsolutions of albite from ternary feldspar – intra- and extragranular (sample UK1). **c)** Large perthitic K-feldspars (light gray) in UK1 associated with interstitial grains of plagioclase (darker gray). **d)** Blown up portion of the Fig. 3c with zoned plagioclase grain featuring albitic rim (darker) and oligoclase core (lighter gray).

tres thick, conformable to the foliation of the surrounding felsic calc-alkaline Ky–Grt granulites (Fig. 2b).

4.1.1. Alkali feldspar

The bulk of the rock consists of mostly perthitic K-feldspar (microcline). It shows several hues of a bright blue luminescence, which is typical of most alkali feldspars (Fig. 2c–d, f, h). The favoured mechanisms triggering this CL are activation by Ti^{4+} ions or the presence of defects in the crystal lattice, namely holes on Al^{3+}–O^{2+}–Al^{3+} (Löwenstein) bridges (Geake et al. 1977; Marshall 1988; Finch and Klein 1999; Götze et al. 1999, 2000).

All the K-feldspars are similar to each other in terms of their appearance and composition (Tab. 2, Fig. 3). They tend to be patchy zoned, with darker (BSE, Fig. 3a) patches being higher in Na_2O (up to 1.6 wt. % Na_2O). The barium remains very constant throughout the grains regardless of their internal structure (0.14–0.26 wt. %); also the phosphorus contents are low (P_2O_5 < 0.08 wt. %).

The albitic plagioclase exsolves from the ternary feldspars, forming fine perthites (Fig. 3a–c, CaO < 0.5 wt. %); extragranular exsolution (along grain interfaces, Fig. 3c–d) is also common. Moreover, there occur larger interstitial grains with comparably An-rich cores (Fig. 3d, up to 5 wt. % CaO) and albitic rims.

4.1.2. Garnet

The hyperpotassic granulites contain a variable amount of garnet, several mm–1 cm across, dominated by almandine and pyrope ($Alm_{56.4–65.2}$, $Prp_{22.1–28.2}$, $Grs_{10.0–14.8}$, $Sps_{1.7–2.5}$ mol. %; Tab. 3). This garnet contains a significantly higher *Prp* proportion than the first generation of (HP) garnet in the associated calc-alkaline granulites (Vrána 1989). The high *Grs* component in garnets from both granulite

Tab. 3 Selected garnet, rutile, ilmenite and titanite analyses

Plešovice type – garnet

	Grt A	Grt E	Grt F	Grt G	Grt H	Grt I	Grt J
Sample	UK3	UK3	UK3	UK3	UK3	UK3	UK3
Desc	Large, core	Core	Rim	Core	Rim	Core	Rim
SiO_2	38.56	38.71	38.32	38.75	38.22	38.25	38.38
TiO_2	0.08	0.01	0.01	0.12	0.04	0.05	0.08
Al_2O_3	22.06	22.20	21.85	21.94	21.87	21.59	21.80
FeO	25.88	28.38	28.86	25.59	29.04	27.79	27.49
MnO	0.77	1.03	1.11	0.82	1.07	0.95	0.99
MgO	6.95	5.72	5.52	7.18	5.59	5.59	5.31
CaO	4.57	4.21	3.71	4.82	3.46	4.94	5.15
P_2O_5	0.08	0.02	0.02	0.17	0.01	0.04	0.04
Total	98.95	100.28	99.39	99.40	99.29	99.19	99.24
Alm	57.64	63.04	64.74	56.36	65.23	61.69	61.69
Prp	27.59	22.66	22.07	28.20	22.39	22.13	21.25
Grs	13.03	11.99	10.67	13.60	9.95	14.04	14.81
Sps	1.74	2.31	2.52	1.84	2.43	2.14	2.25

Plešovice type – rutile and ilmenite

	Rt K	Rt M	Rt 2 + Grt	Rt 2*	Rt 5 + Grt	Rt 5*	Ilm 3	Ilm 3*
Sample	UK1	UK1	UK3	UK3	UK3	UK3	UK3	UK3
Desc	Cores, large grains in Bt		Unmixed from Grt		Unmixed from Grt		Unmixed from Grt	
SiO_2	0.00	0.17	14.90	0.00	20.67	0.00	21.97	0.00
TiO_2	94.74	99.55	59.89	95.25	43.55	98.04	22.98	53.78
Al_2O_3	0.10	0.16	8.95	0.68	11.71	-0.26	12.79	0.51
FeO	–	–	11.34	2.13	14.02	0.32	34.10	45.29
MnO	–	–	0.35	0.08	0.37	-0.10	0.58	0.33
MgO	–	–	2.78	0.15	3.67	-0.12	4.67	1.66
CaO	0.00	0.00	1.89	0.20	2.41	-0.09	1.93	-1.57
Nb_2O_5	2.03	0.27	0.02	b.d.	b.d.	b.d.	b.d.	b.d.
ZrO_2	1.09	0.35	0.95	1.51	0.98	2.21	0.00	0.00
HfO_2	0.21	0.18	b.d.	b.d.	b.d.	b.d.	b.d.	b.d.
Total	98.17	100.69	101.07	100.00	97.38	100.00	99.02	100.00

Lhotka type – Ti minerals

	Titanite (12/6h)[a]	Pseudorutile (13/6h)	Ti-phase (14/6h)	Ti-phase (15/6g)
Sample	UK5	UK5	UK5	UK5
Desc	Within Amph	Within Amph	Within Amph	Within Amph
SiO_2	29.05	1.81	11.84	20.63
TiO_2	36.43	62.23	74.72	17.48
Al_2O_3	0.18	0.04	0.48	2.29
FeO	1.56	19.70	3.28	7.26
MnO	b.d.	0.33	0.00	0.00
MgO	b.d.	b.d.	b.d.	0.41
CaO	28.84	2.05	0.98	6.13
ZrO_2	1.24	0.26	0.98	3.04
HfO_2	0.39	0.31	0.51	0.57
Cr_2O_3	0.54	1.03	1.39	4.57
ΣREE_2O_3	1.67	2.47	3.23	29.27
Y_2O_3	0.87	1.58	0.78	0.37
Na_2O	0.18	0.14	0.06	0.44
Total	100.96	91.97	98.26	[b]95.03

b.d.: below detection limit (see Table 1)

* recast to 100 wt. % after subtraction of garnet Grt A

[a] analysis in Fig. 6; [b] including 1.89 wt. % P_2O_5 and 0.69 wt. % ThO_2

types would theoretically point to relatively high equilibration pressures. However, this mineral and apatite are the only Ca sinks in the hyperpotassic granulites. In the absence of plagioclase, the Ca contents in the garnet are thus not buffered and may not reflect the pressure of crystallization at all. The phosphorus contents are generally low, reaching a maximum of 0.72 wt %, i. e. 0.011 apfu.

The crystals are continuously zoned, with *Alm* and *Sps* components increasing at the expense of *Prp* in a narrow zone close to the rims. The *Grs* component is either nearly constant or shows a slight decrease towards the rim. This is in contrast to the common calc-alkaline granulites, whose *Grs*-rich (HP) garnet cores grade to relatively *Grs*-poor rims and where even occurs the second, *Grs*-poor garnet generation.

Most garnets contain inclusions of apatite, zircon. rutile and, or, ilmenite. Some of the samples

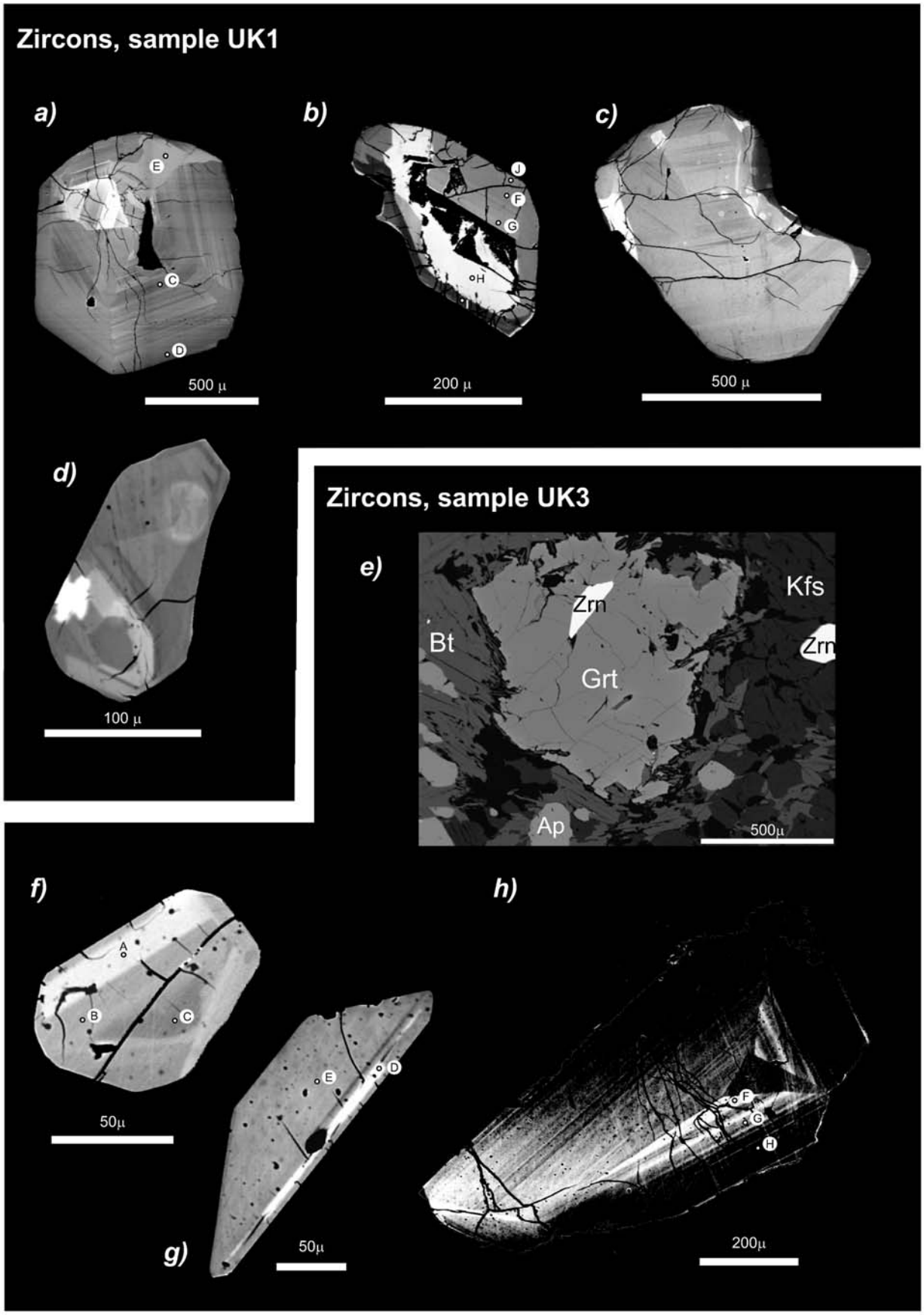
Zircons, sample UK1
a)
E
C
D
500 μ
b)
J
F
G
H
I
200 μ
c)
500 μ
d)
100 μ
Zircons, sample UK3
e)
Zrn
Kfs
Bt
Zrn
Grt
Ap
500μ
f)
A
B
C
50μ
E
D
g)
50μ
h)
F
G
H
200μ

show effects of retrogression, with garnet breaking down to biotite (Fig. 2e–h). The process starts typically at rims (Fig. 2e–f) and along cracks (Fig. 2g–h). However, in the quarry one can find mafic and biotite-rich granulite gneisses, in which the transformation was nearly complete. Primary quartz is mostly missing, even though hyperpotassic granulites in the Plešovice quarry are accompanied by less common, garnet-bearing, zircon-rich granulites of alkali feldspar granite composition (Vrána 1989). In the ordinary alkali feldspar syenitic granulites, some secondary quartz originated through garnet breakdown as did plagioclase, a primary generation of which is also absent (see Vrána 1989 for details). Sodic plagioclases with quartz form often a symplectite at the garnet–biotite boundaries suggesting a reaction Grt + Kfs = Pl + Bt + Qtz (Fig. 2g–h).

4.1.3. Zircon

Many of the hyperpotassic granulites are characterised by macroscopically apparent, mostly euhedral and equant zircon grains, several mm across. According to Vrána (1989), these zircons have morphology typical of alkaline magmatic rocks (Pupin 1980).

Zircon shows very weak luminescence as confirmed by both optical (Fig. 2d) and SEM-mounted CL systems. However, characteristic is a well-developed zoning apparent under optical microscope and in the BSE. Conspicuous oscillatory zoning is common (e.g., Figs 4a, h), with a variable but lesser role for sector zoning (Figs 4c–d). Late seem to be patches with high BSE intensity (light grey–whitish), which obscure the primary igneous zoning (Figs 4a–d). In some grains these patches become rather important (Fig. 4b). Even though the great majority of zircons occurs in the K-feldspar matrix or in clusters at margins of large garnet crystals, some of them form inclusions in garnet grains (Fig. 4e), with a shape and position suggesting heterogeneous nucleation at the crystallizing garnet surfaces. The initial contact plane is often marked by an eye-catching bright (BSE) zone (Fig. 4f–g).

The electron microprobe analyses (Tab. 4) reveal that the intensity of the BSE signal is correlated with increasing contents of uranium (up to 0.26–0.40 wt. % of UO_2, 0.02–0.003 U apfu). While the contents of HfO_2 change in a rather erratic manner between 1.70 and 2.55 wt. %, the incorporation of U into the crystal lattice seems to be accompanied by increased contents of P_2O_5, ThO_2 and Y_2O_3. An increase in mean atomic number (and thus also the BSE intensity) due to elevated contents of U, Th, Hf and HREE was assumed by number of authors (e.g., Benisek and Finger 1993; Hanchar and Miller 1993; Corfu et al. 2003; Nasdala et al. 2003) but this does not need to be the case if vacancies or H_2O are present in the crystal lattice (Kempe et al. 2000; Nasdala et al. 2003).

Keeping in mind the limited size of the available data set, there seem to be no systematic differences in zircon chemistry between the large crystals in the matrix and inclusions within the garnet. The only exception may be Fe, which is slightly elevated (0.004–0.010 apfu) in the inclusions. However, contamination by the adjacent garnet in these cases cannot be ruled out due to the limited size of the inclusions.

4.1.4. Apatite

Abundant apatite (up to several vol. %) forms mostly oval grains up to several mm across, often gathering in conspicuous clusters or linear chains. The apatite is characterised by a striking continuous rimward zoning observable both in CL and, to some extent, the BSE. In many of the grains the luminescence changes at the grain boundaries and along cracks from dull orange (bright BSE) to much brighter yellow (darker BSE) (Figs 2c, f, 5c–d). The apatite grains featuring duller zones are often associated with small anhedral grains of monazite at their rims (e.g., Figs 5a, c–d). Apatite grains lacking monazite tend to a brighter BSE signal (e.g., the grain labelled in Fig. 5a). No oscillatory zoning typical of some magmatic apatites (Dempster et al. 2003) was observed.

The composition of analysed grains (Tab. 5) corresponds to a rather pure fluor-apatite, the Cl contents being below 0.2 wt. % in all cases. However some differences do exist; the apatites with lower intensity of the BSE signal (dull grains and rims of zoned crystals) show much lower LREE contents (see analyses ap3, ap7). Less apparent but still significant seem to be their decreased contents of Mg, Fe and Na. The Mn and Y are constantly low, Sr does not exceed detection limit for any of the analysed spots.

The bright yellow luminescence typically observed in apatite from igneous rocks is believed to having been triggered by trace amounts of Mn (Marshall 1988). However presence of various REE and Fe is assumed to be effective in its quenching (Mitchell et al. 1997; Kempe and Götze 2002; Waychunas 2002). The Mn contents in the Plešovice apatites are uniformly low and recognition of subtle differences may be beyond the capabilities of the electron microprobe. Still, the elevated contents of LREE and some other atoms in grains/parts thereof showing dull luminescence (and bright BSE signal) may indicate their possible quenching effects.

⇐

Fig. 4 BSE images of zircon crystals from the samples UK1 (a–d) and UK3 (e–h). They show well developed oscillatory zoning, with a few bright patches rich in U. Locations of analytical points (see Tab. 4) are marked by small letters. Figure 4e outlines position of the analysed grain (g) in garnet, surrounded by K-feldspar, apatite and secondary biotite.

Tab. 4 Selected zircon analyses recalculted on the basis of 4 O

Plešovice type

Sample	UK1/C	UK1/D	UK1/E	UK1/F	UK1/G	UK1/H	UK1/I	UK1/J
BSE fig	Fig 4a	Fig 4a	Fig 4a	Fig 4b	Fig 4b	Fig 4b	Fig 4b	Fig 4b
Description	Oscillatory zoning			Complex discontinous zoning				
SiO_2	33.13	33.19	32.63	32.46	32.55	32.56	32.57	31.87
ZrO_2	65.14	65.05	65.80	66.08	65.99	65.61	65.57	66.47
HfO_2	1.88	1.89	1.83	1.72	1.69	1.71	1.80	1.72
UO_2	0.05	0.06	0.11	0.09	0.14	0.32	0.05	0.11
ThO_2	0.00	0.00	0.04	0.00	0.02	0.07	0.02	0.02
FeO	–	–	–	–	–	–	–	–
Nb_2O_5	0.09	0.00	0.07	0.03	0.03	0.02	0.00	0.00
P_2O_5	0.04	0.01	0.08	0.10	0.09	0.12	0.03	0.10
Y_2O_3	0.01	0.04	0.10	0.07	0.09	0.12	0.01	0.10
Total	100.35	100.24	100.67	100.55	100.58	100.54	100.05	100.38
Zr	0.969	0.969	0.981	0.986	0.984	0.979	0.982	0.998
Hf	0.016	0.017	0.016	0.015	0.015	0.015	0.016	0.015
Fe	0.000	0.000	0.000	0.000	0.000	0.000	0.000	0.000
Nb	0.001	0.000	0.001	0.000	0.000	0.000	0.000	0.000
Th	0.000	0.000	0.000	0.000	0.000	0.001	0.000	0.000
U	0.000	0.000	0.001	0.001	0.001	0.002	0.000	0.001
Y	0.000	0.001	0.002	0.001	0.001	0.002	0.000	0.002
Σ	0.988	0.986	1.000	1.003	1.002	0.999	0.999	1.016
Si	1.011	1.014	0.997	0.993	0.996	0.997	1.001	0.981
P	0.001	0.000	0.002	0.003	0.002	0.003	0.001	0.003
Σ	1.012	1.014	0.999	0.996	0.998	1.000	1.001	0.984

Plešovice type

Analysis	UK3/A	UK3/B	UK3/C	UK3/D	UK3/E	UK3/F	UK3/G	UK3/H
BSE fig	Fig. 4f	Fig. 4f	Fig. 4f	Fig. 4g	Fig. 4g	Fig. 4h	Fig. 4h	Fig. 4h
Description	Inclusion in Grt			Inclusion in Grt		Oscillatory zoning		
SiO_2	33.06	33.31	33.04	33.00	33.05	32.88	33.11	33.03
ZrO_2	63.93	63.80	64.06	64.06	63.81	64.91	64.87	64.51
HfO_2	1.70	2.30	1.80	2.11	1.89	2.28	2.55	2.40
UO_2	0.40	0.13	0.05	0.26	0.13	0.10	0.10	0.08
ThO_2	0.07	0.02	0.00	0.02	0.01	0.00	0.00	0.00
FeO	0.31	0.26	0.34	0.40	0.15	0.00	0.02	0.00
Nb_2O_5	0.20	0.18	0.16	0.17	0.19	0.21	0.15	0.19
P_2O_5	0.12	0.07	0.01	0.09	0.07	0.05	0.06	0.04
Y_2O_3	0.11	0.05	0.00	0.14	0.06	0.04	0.00	0.00
Total	99.89	100.13	99.46	100.26	99.35	100.48	100.87	100.26
Zr	0.956	0.951	0.960	0.956	0.957	0.968	0.964	0.963
Hf	0.015	0.020	0.016	0.018	0.017	0.020	0.022	0.021
Fe	0.008	0.007	0.009	0.010	0.004	0.000	0.000	0.000
Nb	0.003	0.003	0.002	0.002	0.003	0.003	0.002	0.003
Th	0.001	0.000	0.000	0.000	0.000	0.000	0.000	0.000
U	0.003	0.001	0.000	0.002	0.001	0.001	0.001	0.001
Y	0.002	0.001	0.000	0.002	0.001	0.001	0.000	0.000
Σ	0.986	0.982	0.988	0.992	0.983	0.992	0.989	0.987
Si	1.014	1.018	1.016	1.010	1.017	1.006	1.009	1.011
P	0.003	0.002	0.000	0.002	0.002	0.001	0.002	0.001
Σ	1.017	1.020	1.016	1.013	1.019	1.007	1.010	1.012

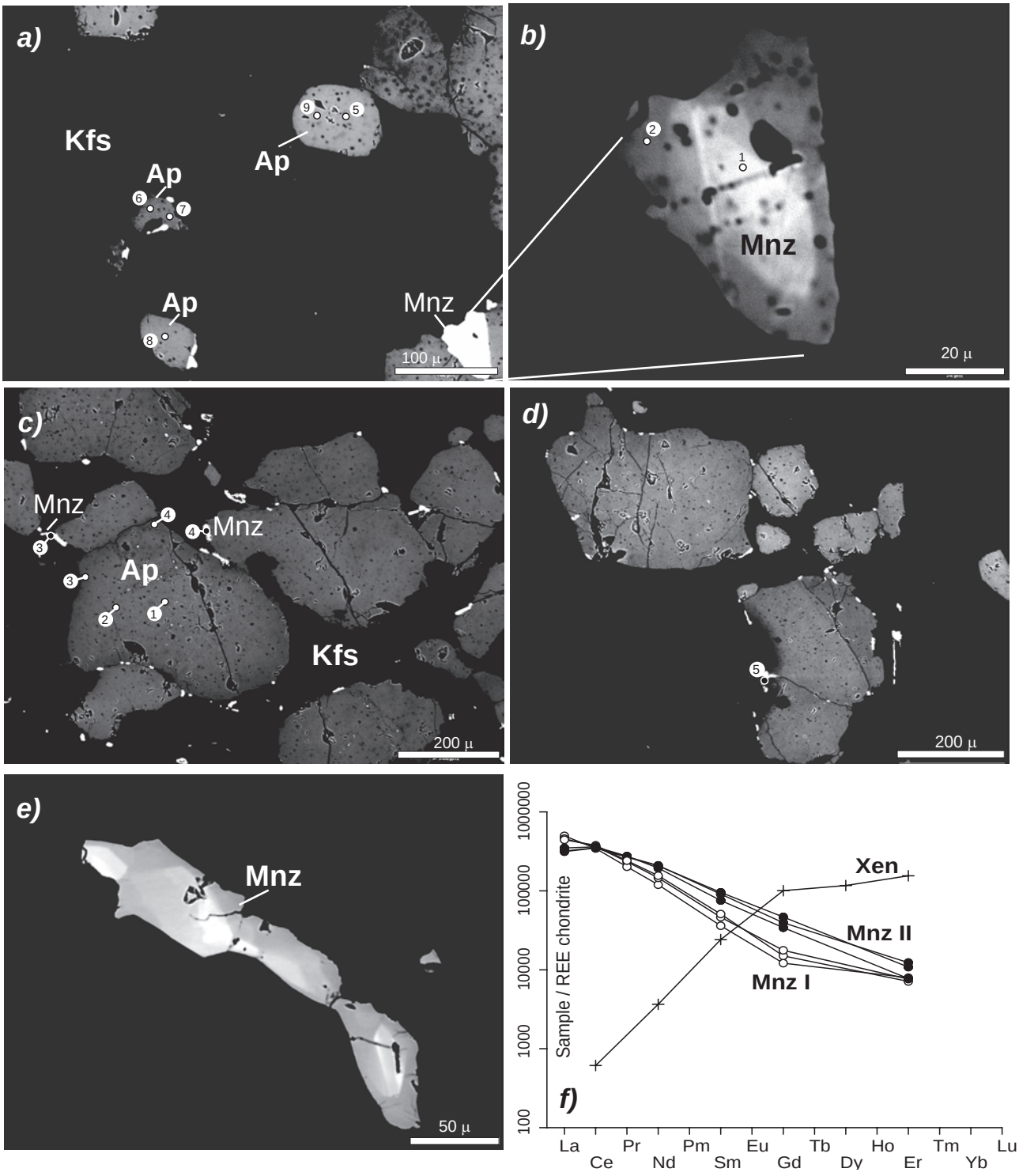

Fig. 5 BSE images of apatite and monazite in the sample UK3 (a–c, e) and UK1 (d), showing faint zoning in the apatite crystals and distribution of the secondary monazite. Analytical points in apatite (Tab. 5) and monazite (Tab. 6) are marked by small numbers. The monazite (e) is a detail of monazite from Fig. 2d. **f** Chondrite-normalized (Boynton 1984) REE patterns for monazite, both primary (Mnz I) and secondary (Mnz II). Xen = secondary xenotime, associated with biotite inclusion, both having originated by a breakdown of the surrounding garnet.

4.1.5. Monazite and xenotime

Two monazite generations can be distinguished: (1) rather rare early, larger grains enclosed in K-feldspar or garnet (Figs 5a–b), and (2) abundant secondary, small grains occurring mostly interstitially or at margins of the apatite clusters (Figs 5a, c–d). However many of the apatites are,

Tab. 5 Selected apatite analyses recalculted on the basis of 12.5 O

	Plešovice type				*Lhotka type*		
Analysis	UK3/ap1	UK3/ap3	UK3/ap5	UK3/ap7	UK5 /ap7	UK5/ap8	UK5/ap9
BSE fig	Fig. 5c	Fig. 5c	Fig. 5a	Fig. 5a	Fig.6e	Fig. 6e	Fig. 6e
Description	Large zoned Ap (core/rim)		Smaller unzoned grain bright BSE. No Mnz	Small grain with admixed Mnz. Dark BSE	Large zoned Ap		
Na_2O	0.19	0.10	0.13	0.06	0.11	0.17	0.18
CaO	54.65	55.02	55.48	55.10	55.27	54.40	53.75
MgO	0.06	0.02	0.07	0.02	b.d.	b.d.	b.d.
MnO	0.07	0.09	0.06	0.03	b.d.	b.d.	b.d.
FeO	0.23	0.09	0.32	0.16	b.d.	b.d.	b.d.
La_2O_3	0.18	0.00	0.10	0.05	0.07	0.14	0.14
Ce_2O_3	0.39	0.14	0.36	0.14	0.17	0.34	0.51
Pr_2O_3	0.11	0.04	0.12	0.00	0.00	0.00	0.00
Nd_2O_3	0.27	0.10	0.22	0.11	0.12	0.33	0.36
Sm_2O_3	0.07	0.04	0.04	0.03	0.00	0.00	0.00
Gd_2O_3	0.00	0.42	0.12	0.09	0.00	0.00	0.00
Dy_2O_3	0.00	0.00	0.02	0.00	0.00	0.00	0.00
Er_2O_3	0.26	0.12	0.10	0.24	0.00	0.00	0.00
Y_2O_3	0.11	0.10	0.10	0.12	0.17	0.19	0.26
SiO_2	0.09	0.19	0.10	0.03	0.03	0.22	0.35
P_2O_5	42.03	42.21	41.82	42.21	40.13	39.87	39.19
TiO_2	0.00	0.03	0.02	0.05	n.d.	n.d.	n.d.
ThO_2	0.00	0.03	0.04	0.00	0.01	0.06	0.00
UO_2	0.00	0.00	0.01	0.02	0.00	0.00	0.00
Total	98.72	98.73	99.23	98.45	[a]99.65	[b]99.23	[c]98.43
Na	0.031	0.016	0.021	0.009	0.018	0.027	0.028
Ca	4.913	4.928	4.973	4.947	4.968	4.918	4.913
Mg	0.008	0.002	0.009	0.002	–	–	–
Mn	0.005	0.006	0.005	0.002	–	–	–
Fe	0.016	0.007	0.022	0.011	–	–	–
La	0.005	0.000	0.003	0.002	0.002	0.004	0.005
Ce	0.012	0.004	0.011	0.004	0.005	0.010	0.016
Pr	0.003	0.001	0.004	0.000	0.000	0.000	0.000
Nd	0.008	0.003	0.007	0.003	0.004	0.010	0.011
Sm	0.002	0.001	0.001	0.001	0.000	0.000	0.000
Gd	0.000	0.012	0.003	0.003	0.000	0.000	0.000
Dy	0.000	0.000	0.001	0.000	0.000	0.000	0.000
Y	0.005	0.005	0.005	0.005	0.007	0.009	0.012
Σ	5.009	4.984	5.064	4.989	5.004	4.979	4.985
P	2.985	2.988	2.962	2.994	2.993	2.991	2.972

[a] incl. 3.45 wt.% F. 0.11 wt.% Cl; [b] incl. 3.36 wt.% F. 0.15 wt.% Cl; [c] incl. 3.53 wt.% F. 0.11 wt.% Cl

at a closer look, peppered by innumerable tiny (several microns-sized) monazite grains.

The first monazite generation is characterized by discontinuous zoning, with the centres showing much brighter BSE signal. They contain comparably high ThO_2 (~ 3.8 wt. %: mon1 in Tab. 6) and UO_2 (~ 0.8 wt. %). The zoning is related to the drop in concentrations of these oxides (to ~ 0.3 and 0.4 wt %, respectively; see analysis mon2 in Tab. 6), compensated by an increase in MREE contents.

The secondary grains associated with apatite (Fig. 5e) are chemically distinct, and show an extremely low ThO_2 (< 0.1 wt. %) at UO_2 contents of 0.16–0.20 wt. %, (Tab. 6, analyses mon3–5; Fig. 5c–d). On the other hand, the MREE contents are higher than in the primary monazites (Fig. 5f). The somewhat elevated Ca contents in some of the grains are probably due to contamination by the adjacent apatite as they are in excess of the stoichiometrically required amount (Th + U = Si + Ca).

Tab. 6 Selected monazite analyses recalculted on the basis of 16 O

	Plešovice type						*Lhotka type*	
Analysis	UK3/mon1	UK3/mon2	UK3/mon3	UK3/mon4	UK3/mon5	UK3/mon6	UK5/mon10	UK5/mon11
BSE fig	Fig. 5b	Fig. 5b	Fig. 5c	Fig. 5c	–	–	Fig. 6f	Fig. 6f
Description	Large zoned Mnz (core/rim)		unmixed from Ap	unmixed from Ap	unmixed from Ap	large unzoned Mnz in Grt	zoned Mnz at apatite rim	zoned Mnz at apatite rim
SiO_2	0.49	0.04	0.06	0.03	0.00	0.02	0.08	0.27
P_2O_5	28.75	29.86	29.27	29.62	29.70	29.83	29.94	28.93
CaO	0.62	0.30	*0.14*	*0.63*	*0.32*	0.15	0.16	0.22
SrO	0.07	0.08	0.08	0.05	0.07	0.05	< d.l.	< d.l.
La_2O_3	18.10	16.68	12.69	11.63	11.42	16.11	21.08	18.65
Ce_2O_3	32.59	34.46	34.11	33.18	32.94	35.74	34.21	32.23
Pr_2O_3	2.88	3.34	3.93	3.86	3.82	3.45	3.20	3.57
Nd_2O_3	8.37	10.24	13.60	14.66	14.50	10.90	(1) 8.70	(2) 9.52
Sm_2O_3	0.82	1.05	1.71	2.06	2.16	1.15	0.89	1.06
Gd_2O_3	0.36	0.53	1.02	1.18	1.39	0.45	0.31	0.32
Dy_2O_3	0.03	0.10	0.12	0.21	0.25	0.08	0.15	0.02
Er_2O_3	0.19	0.18	0.19	0.30	0.26	0.17	< d.l.	< d.l.
Y_2O_3	0.37	0.54	0.82	1.15	1.33	0.46	0.29	0.42
ThO_2	3.77	0.32	0.00	0.00	0.00	0.11	0.34	2.39
UO_2	0.79	0.42	0.16	0.20	0.18	0.50	0.15	0.21
Total	98.22	98.14	97.90	98.76	98.35	99.17	(a) 99.91	(b) 97.99
Si	0.079	0.007	0.010	0.005	0.000	0.004	0.013	0.043
P	3.911	4.012	3.975	3.974	3.995	3.993	3.953	3.929
Σ	3.990	4.019	3.986	3.978	3.995	3.996	(a)4.011	(b)3.992
Ca	0.108	0.051	*0.025*	*0.108*	*0.055*	0.025	0.027	0.039
Sr	0.007	0.007	0.007	0.005	0.007	0.005	0.000	0.000
La	1.072	0.976	0.751	0.680	0.669	0.940	1.212	1.104
Ce	1.917	2.002	2.004	1.925	1.916	2.068	1.952	1.894
Pr	0.169	0.193	0.230	0.223	0.221	0.199	0.182	0.209
Nd	0.480	0.580	0.779	0.830	0.823	0.615	0.485	0.546
Sm	0.045	0.057	0.094	0.112	0.118	0.063	0.048	0.059
Gd	0.019	0.028	0.054	0.062	0.073	0.023	0.016	0.017
Dy	0.002	0.005	0.006	0.011	0.013	0.004	0.007	0.001
Er	0.010	0.009	0.009	0.015	0.013	0.008	0.000	0.000
Y	0.031	0.045	0.070	0.097	0.112	0.038	0.024	0.036
Th	0.138	0.012	0.000	0.000	0.000	0.004	0.012	0.087
U	0.028	0.015	0.006	0.007	0.006	0.018	0.005	0.007
Σ	4.026	3.982	4.036	4.073	4.026	4.010	3.970	3.999

(1) La/Nd = 2.42; (2) La/Nd = 1.96

(a) incl. 0.39 wt.% SO_3/0.045 S pfu; (b) incl. 0.17 wt.% SO_3/0.020 S pfu

The low Th contents, the enrichment in MREE and the textural relationships strongly suggest that this monazite generation formed using components from the apatite. This idea is also supported by the mineral chemistry of apatite grains occurring in a close association with the monazite. As noted above, the apatite is, at margins and along cracks, notably impoverished in LREE.

Another REE phosphate is xenotime that occurs exclusively associated with secondary biotite and biotite-filled cracks, penetrating the garnet grains. Its origin is clearly related to Y + HREE released by the garnet breakdown.

4.1.6. Fe–Ti oxides

Rutile occurs in two generations. One is represented by larger grains, often subhedral/euhedral, in the K-feldspar or biotite matrix. The second is hosted in garnet in form of numerous tiny isometric grains or, in some samples, needles oriented along crystallographically controlled planes. A part of the small grains enclosed in garnet were shown to be ilmenite.

Some of the rutiles in the matrix are relatively rich in Zr and Nb, reaching ~1.0 wt. % of ZrO_2 and ~1.7–2.0

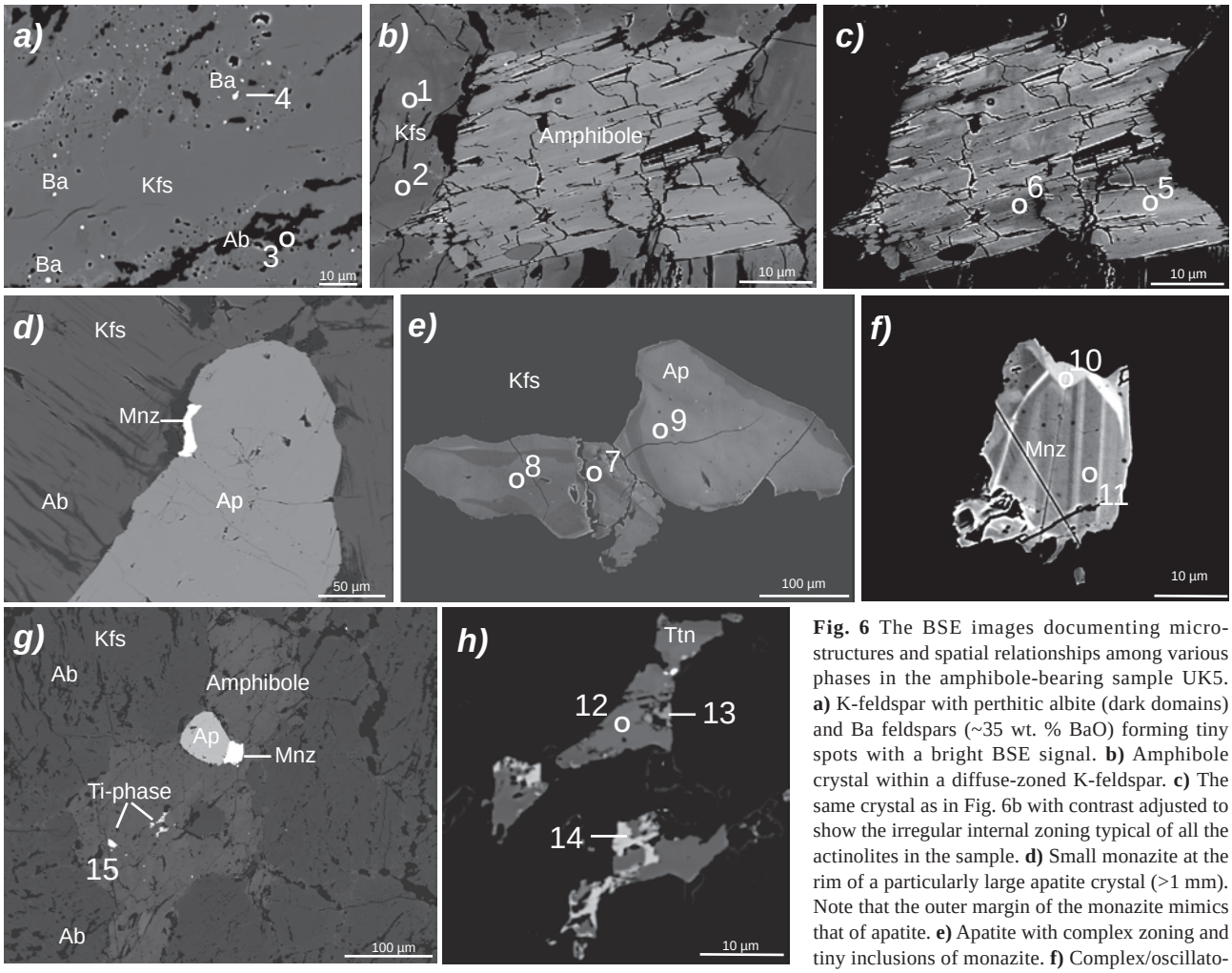

Fig. 6 The BSE images documenting microstructures and spatial relationships among various phases in the amphibole-bearing sample UK5. **a)** K-feldspar with perthitic albite (dark domains) and Ba feldspars (~35 wt. % BaO) forming tiny spots with a bright BSE signal. **b)** Amphibole crystal within a diffuse-zoned K-feldspar. **c)** The same crystal as in Fig. 6b with contrast adjusted to show the irregular internal zoning typical of all the actinolites in the sample. **d)** Small monazite at the rim of a particularly large apatite crystal (>1 mm). Note that the outer margin of the monazite mimics that of apatite. **e)** Apatite with complex zoning and tiny inclusions of monazite. **f)** Complex/oscillatory-like zoning in monazite. Detail of the Fig. 6g. **g)** Large actinolite crystal with Ti phases and an apatite–monazite intergrowth. **h)** Detailed image of the Ti-rich inclusions from 6g. Distinct shades of gray correspond to various Ti phases (Tab. 3).

wt. % of Nb_2O_5 (Tab. 3). The others show much lower ZrO_2 and Nb_2O_5 contents (close to 0.3 wt. % each). The most likely explanation is that all the rutiles were initially Zr–Nb rich and the observed non-systematic differences are connected to diffusional resetting upon cooling (Zack et al. 2004). The lack of quartz prevents the Zr in rutile thermometry of Zack et al. (loc. cit.) to be applied and seems to be the prime cause for unusually high Zr contents many of the Plešovice rutiles (Zack 2004, pers. comm.).

The chemistry of the inclusions in garnet can be only estimated, as the electron microprobe spots are too large and contamination by the matrix seems inevitable. For this reason, an attempt was made to strip the garnet component from the analyses assuming that all silica belongs to garnet of composition similar to the analysis UK3/A. After normalizing to 100 % a rough estimate of the Fe, Ti and Zr proportions can be made (Tab. 3, labelled by asterisks). The concentration of ZrO_2 seems to be even higher than in the rutiles from the matrix, ranging between *c.* 1.5 and 2.2 wt. %. However, no Nb was detected. In Tab. 3 is also presented a typical composition one of the ilmenite inclusions – all of them seem to be Zr and Nb free, despite the fact, that some ilmenites may be rather Zr-rich and their breakdown may even lead to formation of zircon (Bingen et al. 2001).

The chemistry of the studied rutile inclusions argues stoutly for their origin by unmixing from the garnet solid solution. It is well known that garnet can represent an important reservoir for Zr in high-grade metamorphic rocks (e.g., Fraser et al. 1997; Degeling et al. 2001; Rubatto 2002) and the Zr contents in the garnets of the hyperpotassic Plešovice granulites indeed are rather high (35–85 ppm according to Sláma 2006, pers. comm.). This may explain the elevated Zr contents observed in the rutile inclusions. On the other hand, the inclusions show negligible concentrations of Nb, an element incompatible with the garnet crystal lattice. Inclusions of rutile, very often in the form of acicular crystallographically oriented crystals, are assumed to form upon decompression and/or

cooling of high-grade metamorphic terranes (Donohue et al. 2001; Zhang et al. 2003). The high Ti solubility in the garnet lattice at high temperatures and its exsolution due to cooling in the form of oriented rutile needles has been further supported by experiments concerned with the petrogenesis of the Moldanubian granulites (Tropper et al. 2005).

4.2. Pyroxene/actinolite-bearing hyperpotassic granulites (Lhotka type)

Within the central part of the BLGM (on a hillock 300–400 m SW of Lhotka, 2.5 km W of Křemže) another occurrence of hyperpotassic granulites has been described, which are not garnet- but pyroxene-bearing (Vrána 1998). An up to ~15 m thick tabular body of the hyperpotassic pyroxene granulite is surrounded by ordinary, felsic calc-alkaline Grt–Ky granulites. The rock is dominated by perthitic K-feldspar (estimated modal proportion 85–90 vol. %) with a limited amount of unmixed albite (5–10 %). The other components are quartz (~1–5 %), apatite (~1–3 %), Fe-sulphides/oxides (<1 %) and Ba-feldspar (<1 %). The ferromagnesian minerals are represented by up to several % of poikilitic pyroxene and products of its decomposition; no garnet was found. The diopside is often replaced by secondary actinolite (Vrána 1998), as in the newly collected sample UK5, which seems to lack any traces of the primary pyroxene.

The apatites are variable in size (reaching 1 mm or more), looking similar as in the Plešovice hyperpotassic granulites (clusters of subhedral/round grains). No zircon was found in the sample UK5, albeit Vrána (1998) reported from his samples equant zircons up to 3 mm in diameter. The other accessories include monazite, Ti phases and, locally, allanite.

4.2.1. Feldspars

The K-feldspar, whose chemical composition is characterised by high Ba concentrations (~0.5–0.6 wt. % BaO), always shows a diffuse, patchy-like zoning (Fig. 6b). Systematically higher Na abundances were found in the darker domains (~0.4–1.5 wt. % Na_2O, see analyses UK5/1 and 2 in Tab. 2). Furthermore the K-feldspar looks rather fragmented as abundant cracks, holes and domains with unmixed albite patches of variable size and shape are present (e.g. Fig. 6a, g). Modal abundances of up to ~10 % of perthite albite, which have been deduced from the whole-rock geochemistry, are in a good agreement with their frequent occurrence revealed by the BSE. The unmixed albite is poor in calcium (<<0.1 wt. % CaO), potassium (<<0.1 wt. %) and barium (below detection limit).

As mentioned above, the K-feldspar is extremely rich in Ba and thus accounts for much of the high whole-rock Ba budget (~ 6 300 ppm: UK5). However, this element is not only hosted by the K-feldspar, but also in very high concentrations (~35 wt. % BaO, see Tab. 2, analysis Ba Fsp4) in numerous tiny (<<5 μm), round to oval Si- and Al-rich grains with a very bright BSE signal (of intensity comparable to zircon). Even though the grains are too small to obtain pure, uncontaminated analyses, the high Ba values and a plagioclase-like Ba–Si–Al stoichiometry suggest them to be celsians, i.e. Ba-feldspar *sensu stricto* (Deer et al. 1992). They probably exsolved from the ternary feldspars, together with the perthite albite. This is in line with the observation that some of such Ba grains are enclosed within the unmixed albite patches.

The extremely low Ca contents in the plagioclase may be ascribed either to the low whole-rock Ca concentrations or, alternatively, to the possibility of this element having been exhausted by the growth of other Ca phases (e.g. apatite and/or pyroxene) prior to the onset of the ternary K-feldspar crystallization. The low K concentrations in the K-feldspar perthite host would theoretically indicate low exsolution temperatures, at least in a lower pressures regime (e.g. Smith and Brown 1988). However the measured concentrations in this sample probably do not reflect a primary equilibrated state, as shown by erratically distributed, highly variable Na concentrations in the host K-feldspar.

4.2.2. Pyroxene/amphibole

According to Vrána (1998), the diopside has Mg/(Mg + Fe) = 0.77 and contains 0.8–1.0 wt. % Na_2O. At margins and along cracks it is replaced by secondary amphibole with little biotite. In the newly collected sample UK5 the diopside transformation is complete. In the classification scheme of Leake et al. (1997) its amphibole corresponds to actinolite (Ca_B = 1.86–2.00, $(Na+K)_A$ = 0.21–0.39, Si = 7.70–7.88, Ca_A = 0.00–0.09). The widely scattered, sub- to anhedral amphibole grains are up to *c.* 2 mm across. The secondary formation seems responsible for the diffuse patchy zoning and, in addition, may explain the occurrence of biotite inclusions in this mineral phase. The slight BSE contrasts between adjacent zones can be ascribed to minor variations in Na, Fe, Mg and Ca (~ 0.8–1.4 wt. % Na_2O, 7.1–11.3 wt. % FeO, 16.7–19.5 wt. % MgO). Figure 6c and analyses in the Tab. 7 clearly show that the increase in Fe and Na is compensated by decreasing contents of Mg and Ca in the brighter domains. The other elements like Cr, K and Ti occur commonly in very low concentrations (< 0.3 wt. %); the HREE and Y did not exceed their respective detection limits.

The amphibole crystal in Fig. 6g is of particular interest. It contains not only K-feldspar inclusions, which formed together with, or preceding somewhat, the host actinolite grain. As will be discussed in some detail be-

Tab. 7 Selected amphibole analyses recalculated on the basis of 23 O equivalents

Hyperpotassic granulite UK5 (Lhotka type)

Analysis	Amph 5	Amph 6	Amph D1	Amph D2
BSE fig	Fig. 6c	Fig. 6c	–	–
Description	dark domain	bright domain	dark domain	bright domain
SiO_2	55.00	54.64	55.62	54.11
TiO_2	0.10	0.19	0.04	0.11
Al_2O_3	1.08	1.25	0.75	1.18
FeO	8.58	9.84	7.08	11.26
MnO	0.22	0.22	0.22	0.26
MgO	18.64	18.21	19.46	16.72
CaO	13.85	13.24	13.81	12.33
Cr_2O_3	0.09	0.15	0.06	0.17
K_2O	0.36	0.31	0.39	0.35
Na_2O	0.93	1.22	0.88	1.40
Total	98.85	99.27	98.31	97.91
Si	7.747	7.706	7.814	7.777
Al	0.179	0.208	0.124	0.200
Fe^{II}	1.011	1.161	0.832	1.353
Ti	0.011	0.020	0.004	0.012
Cr	0.010	0.017	0.007	0.019
Mn	0.026	0.026	0.026	0.032
Mg	3.914	3.829	4.076	3.582
Ca	2.090	2.001	2.079	1.899
Na	0.254	0.334	0.240	0.390
K	0.065	0.056	0.070	0.064
$\sum$	15.898	15.934	15.883	15.976
$Mg(Mg+Fe^{II})$	0.795	0.767	0.830	0.726
Ca_A	0.090	0.033	0.079	0.000
Ca_B	2.000	1.968	2.000	1.899
$(Na+K)_A$	0.319	0.389	0.310	0.353

low, this crystal also encloses Ti phases with unusually high concentrations of Zr and REE.

4.2.3. Apatite

Fluorine-rich apatites (3.0–3.6 wt. % F, <0.2 wt. % Cl; including the analyses not given in the Tab. 5) typically form euhedral or subhedral grains, which commonly range in size from a few 100 μm to more than 1 mm. The size, well-developed crystal faces and the fact that inclusions other than monazites are extremely rare or absent probably support an early growth history of this mineral. However, most of the apatite grains reveal a fairly conspicuous discontinuous zoning which, in a few cases such as that shown in Fig. 6e, can become very complex. Here, the randomly distributed domains are also highly variable in size and shape. Occasionally the inner zones with brighter BSE signal are deeply embayed, suggestive of resorption. The zoning is mainly caused by varying abundances of LREE, which range between *c.* 0.3 wt. % in the darkest and 1.5 wt. % in the brightest domains (see analyses UK5/ap7–9, Tab. 5). In the darker areas, the light rare earth elements, concentrations of which are notably low here, are incorporated together with Na. The comparably higher LREE contents in the brighter domains may be related to the fact that – in addition to the Na–LREE substitution – a coupled substitution with Si plays a significant role (e.g. Roeder et al. 1987; Rønsbo 1989; Fleet and Pan, 1995; Fleet et al. 2000). Characteristic of the apatites are their high Nd/La ratios (>1.5), which increase slightly in the brighter domains. Apart from yttrium, which remains, regardless of zoning, relatively constant (~0.2 wt. % Y_2O_3), other elements (Fe, Mg, Mn, Sr, Ba) occur only in insignificant concentrations.

4.2.4. Monazite

Monazites occur exclusively at the rims of, or enclosed within, the apatites (Figs 6d and g). In either case they form small to medium sized (<< 50μm) euhedral or subhedral grains, some of which, as illustrated in Fig. 6f, show a sector-like or weak oscillatory zoning.

Chemically, the monazites can be characterized by their high La/Nd ratios (>2), constantly low Y values (~0.3–0.4 wt. % Y_2O_3) and relatively low but variable contents of actinides (0.2–4.5 wt. % ThO_2, < 0.3 wt. % UO_2). As exemplified by the analyses 10 and 11 (Tab. 6), which correspond to the brightest and darkest domains of the monazite depicted on the Fig. 6f, respectively, the zoning is mainly caused by the variation in actinides. The locally lowered LREE contents might be ascribed to the lattice distortions in Th-rich domains (analysis 11, Tab. 6), which favour the incorporation of smaller (and thus heavier) REE (e.g., Podor and Cuney 1997).

Whereas the low contents of actinides and Y in monazites could be explained by the relatively low whole-rock values (~9 ppm Y, ~3 ppm Th in UK5), the situation looks different for the La/Nd ratios. Given the La/Nd ratio in the whole rock (~1.2), the high monazite ratios (mostly > 2) either mean that the mineral formed together with Nd-rich apatites or exsolved from originally LREE-enriched apatites. The latter scenario, which has been proposed for instance by Finger and Krenn (2007), assumes that granulite-facies apatites can incorporate large amounts of REE at peak metamorphic conditions but release them upon cooling and decompression. This is a synergic effect of fast diffusion rates and lower uptake capacity of the apatite at lower temperatures (Finger and Krenn loc. cit. and references therein). Considering that all monazites occur enclosed in, or in immediate vicinity

Tab. 8a Major- and minor-element whole-rock geochemical analyses of the hyperpotassic granulites from the Blanský les Massif

	BD158	BD159	BD160b	LV122	Fi20/02a	Fi20/02b	Fi21/02	Fi22/02	UK2	UK3	UK5
Locality					Plešovice, quarry						Lhotka
Lab*	CGS	CGS	CGS	CGS	SBG	SBG	SBG	SBG	ACME	ACME	ACME
SiO_2	57.90	56.89	60.46	63.87	61.22	60.77	63.65	61.42	59.77	63.06	63.59
TiO_2	0.12	0.26	0.08	0.06	0.12	0.09	b.d.	0.33	0.07	0.03	0.01
Al_2O_3	16.75	18.20	18.05	18.15	18.22	17.95	18.79	18.32	18.34	17.46	17.50
Fe_2O_3†	0.60	1.43	1.10	0.19	*2.67*	*4.03*	*0.92*	*1.47*	*3.86*	*1.38*	*0.17*
FeO	0.90	5.03	2.41	0.25	–	–	–	–	–	–	–
MnO	0.02	0.11	0.07	b.d.	0.05	0.09	0.01	0.01	0.06	0.02	0.01
MgO	0.49	1.90	0.99	0.17	0.93	1.20	0.42	1.16	1.17	0.48	0.11
CaO	5.13	2.11	1.66	1.04	1.68	1.56	0.80	1.03	1.72	1.08	0.33
Na_2O	1.34	1.99	2.02	1.80	1.78	1.73	1.45	1.47	1.79	1.64	1.49
K_2O	12.20	8.66	10.95	13.89	11.55	10.71	13.30	13.19	11.13	12.24	14.79
P_2O_5	2.76	0.95	0.78	0.62	0.97	0.84	0.56	0.74	0.87	0.68	0.21
CO_2	0.01	0.04	b.d.	0.01	–	–	–	–	–	–	–
H_2O^{+}‡	0.61	1.21	0.74	0.45	*0.54*	*0.61*	*0.71*	*0.79*	*0.50*	*1.00*	*0.60*
H_2O^{-}	0.09	0.13	0.10	0.06	–	–	–	–	–	–	–
F	0.24	0.26	0.16	0.09	0.10	0.11	0.04	0.11	–	–	–
Total	99.16	99.17	99.57	100.65	99.83	99.69	100.65	100.04	99.28	99.07	98.81
mg#	37.8	34.9	34.2	41.9	40.8	37.1	47.5	61.0	37.5	40.8	56.2
A/CNK	0.68	1.10	0.99	0.91	0.99	1.04	1.03	0.99	1.01	0.97	0.92
A/NK	1.09	1.44	1.19	1.01	1.18	1.24	1.12	1.10	1.22	1.09	0.95
K_2O/Na_2O	9.1	4.4	5.4	7.7	6.5	6.2	9.2	9.0	6.2	7.5	9.9

* Laboratories: **CGS:** wet chemical analyses, Czech Geological Survey, Prague; **SBG:** XRF on fused beads, Division of Mineralogy and Material Science, University of Salzburg, Austria; **ACME:** ICP–ES, Acme Analytical Laboratories Ltd., Vancouver, Canada.
† or total iron as Fe_2O_3 (italics)
‡ or loss on ignition (in italics)
'b.d.' below detection limit, '–' not determined
Localities: Plešovice: working quarry, 5 km NE of Český Krumlov
Lhotka: rock outcrop on a small hill, 300–400 m SW of Lhotka, 2.5 km W of Křemže

of, apatite, most of them mimicking the former apatite crystal faces (Fig. 6d), the secondary formation from this mineral is the most likely.

As apatite diffusion is fast at high temperatures, the observed complex apatite zoning should have formed rather late, during uplift-related cooling. Presumably it was the fast cooling rate, which prevented the apatite from attaining the chemical homogenisation.

4.2.5. Titanium phases

The Ti phases, each of which is unusually high in REE, Y and Zr (up to total 30 wt. % REE, 2 wt. % Y_2O_3, 3 wt. % ZrO_2 – see Tab. 3) have been found exclusively within the amphibole shown on Figure 6g. The inclusion, enlarged in Figure 6h, is of particular interest, as it contains not only volumetrically dominant titanite, displaying minor variations in REE, Y and Zr (1–2 wt. % ΣREE, Y_2O_3, ZrO_2, see Tab. 3, analysis Ttn 12) but also a few optically brighter areas. Even though the WDS analyses of these extremely small domains suffer from contamination by the surrounding titanite, they clearly tend to an ilmenite- and rutile-like composition. As these domains are heterogeneous in surface, it is tempting to hypothesize that remnants of titanite, from which these grains most likely formed, are still present. The Mg is low in all analyses suggesting that contamination by surrounding amphibole is negligible. However, compared to titanite, these heterogeneous phases, which are higher in Ca and Ti, respectively are lower in Zr and similar or somewhat higher in Y (see analyses 13 and 14 in Tab. 3).

In some distance from this special mineral assemblage, we could identify other Ti-rich grains, which are spectacularly high in REE (~30 wt. % REE) and Cr (4.6 wt. % Cr_2O_3). Given the moderate to high Si, Ca and Fe contents (20.6 wt.% SiO_2 and 5–10 wt.% of both CaO and FeO), these grains are probably REE (Cr, Fe)-enriched titanite-related phases with X^{2+} (Ca) + X^{4+} (Ti) replaced by 2 X^{3+} (REE, Cr, Fe, Al). This would be in line with the previous literature showing that Ca^{2+} + Ti^{4+} = REE^{3+} + Al^{3+}(and/or Fe^{3+}) is often the dominant substitution mechanism in REE-bearing titanites (e.g. Green and Pearson 1986; Russell et al. 1994; Vuorinen and Hålenius 2005). The coupled exchange via Na (Na + REE = 2 Ca,

Tab. 8b Major- and minor-element whole-rock geochemical analyses of the calc-alkaline granulites from the Blanský les Massif

Locality	BD160a Plešovice	1060	1061	1063	1065	1066	1067	1068	1069	1070
		Holubov, borehole								
Depth (m)	–	1149	1172	1184	1315	1322	1332	1344	1349	1350
Lab*	CGS	CGS	CGS	CGS	CGS	CGS	CGS	CGS	CGS	CGS
SiO_2	76.67	72.72	71.28	75.98	77.70	69.54	62.92	67.00	75.08	76.43
TiO_2	0.08	0.35	0.37	0.14	0.06	0.31	0.99	0.65	0.07	0.07
Al_2O_3	11.67	13.12	13.78	12.40	11.83	15.13	15.50	15.39	13.24	12.18
Fe_2O_3	0.69	0.18	0.08	0.01	0.01	0.18	0.43	0.22	0.14	0.20
FeO	0.98	2.84	2.68	1.53	1.24	2.71	5.43	3.91	1.60	1.34
MnO	0.03	0.05	0.04	0.03	0.02	0.04	0.08	0.05	0.02	0.02
MgO	0.26	1.07	0.77	0.33	0.19	0.99	3.36	1.44	0.50	0.41
CaO	0.65	2.45	2.38	1.38	0.83	3.14	5.52	3.08	1.60	1.11
Na_2O	2.38	3.04	3.65	3.88	3.66	4.36	2.94	3.54	4.74	3.66
K_2O	5.21	3.88	3.99	3.64	4.08	2.18	1.54	3.06	2.15	3.36
P_2O_5	0.14	0.13	0.09	0.04	0.02	0.21	0.21	0.09	0.14	0.13
H_2O^+	0.23	0.09	0.16	0.01	0.11	0.40	0.85	0.68	0.11	0.03
F	0.03	0.05	0.04	0.05	0.02	0.04	0.09	0.03	0.03	0.02
Total	99.02	99.97	99.31	99.42	99.77	99.23	99.86	99.14	99.42	98.96
mg#	22.5	38.9	33.3	27.7	21.3	38.1	50.7	38.5	34.1	32.5
A/CNK	1.09	0.96	0.94	0.97	0.99	0.99	0.94	1.04	1.02	1.04
A/NK	1.22	1.43	1.33	1.20	1.13	1.59	2.38	1.68	1.31	1.26
K_2O/Na_2O	2.2	1.3	1.1	0.9	1.1	0.5	0.5	0.9	0.5	0.9

Locality	1071	1072	1075	1077	1079	1080
	Holubov, borehole					
Depth (m)	1357	1360	1379	1384	1408	1410
Lab*	CGS	CGS	CGS	CGS	CGS	CGS
SiO_2	77.64	72.52	73.21	72.60	65.82	72.58
TiO_2	0.06	0.27	0.21	0.18	0.95	0.26
Al_2O_3	11.62	13.78	13.34	13.55	14.37	13.89
Fe_2O_3	0.01	0.20	0.12	0.15	0.23	0.58
FeO	1.81	1.97	2.28	2.49	5.69	1.16
MnO	0.06	0.03	0.03	0.03	0.07	0.05
MgO	0.29	0.61	0.57	0.84	2.18	0.72
CaO	0.77	1.64	1.56	1.70	3.42	2.37
Na_2O	3.35	3.11	3.23	3.07	2.90	3.42
K_2O	3.06	4.59	4.27	4.32	2.33	4.16
P_2O_5	0.06	0.17	0.19	0.16	0.22	0.09
H_2O^+	0.25	0.48	0.05	0.03	0.90	0.58
F	0.02	0.05	0.07	0.03	0.06	0.05
Total	99.00	99.42	99.13	99.15	99.14	99.91
mg#	22.1	33.6	29.8	36.3	39.7	43.3
A/CNK	1.14	1.05	1.04	1.06	1.06	0.96
A/NK	1.32	1.37	1.34	1.39	1.97	1.37
K_2O/Na_2O	0.9	1.5	1.3	1.4	0.8	1.2

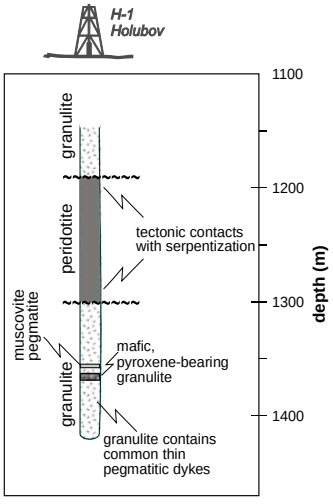

* Laboratories: **CGS:** wet chemical analyses, Czech Geological Survey, Prague.
'b.d.' below detection limit, '–' not determined
Localities: Plešovice: working quarry, 5 km NE of Český Krumlov
Holubov: borehole H-1, 8 km N of Český Krumlov, depth of 1150–1410 m under the surface (see inset)
Additional analyses from the Holubov borehole have been presented by Janoušek et al. (2004).

e.g. Černý et al. 1995; Tiepolo et al. 2002), the second prominent way of REE incorporation in titanites, seems to play a negligible role in this case.

However, all these Ti modifications in UK5 exhibit heterogeneous surfaces with diffuse zoning on a small scale, which makes precise analyses and unambiguous identification very difficult. From textures in combination with chemistry it appears, as if distinct Ti modifications occur intimately intergrown.

5. Whole-rock geochemistry

The newly obtained whole-rock geochemical data for both hyperpotassic and calc-alkaline granulites come from the working quarry in Plešovice, the rock outcrop at Lhotka and the borehole H-1 at Holubov (Kodym et al. 1978; Fediuková 1978) (Tabs 8 and 9). In addition, our database includes the previously presented whole-rock analyses from the BLGM: five hyperpotassic (Strejček 1986; Vrána 1989) and eighty-nine calc-alkaline granulites (Kodym et al. 1978; Slabý 1983; Čadková et al. 1985; Strejček 1986; Fiala et al. 1987a; Gürtlerová et al. 1997; Janoušek et al. 2004). Last but not least, samples BD158, BD159, BD160a, BD160b and LV122 and much of their analyses have been kindly provided by S. Vrána. Data management, recalculation, plotting and statistical evaluation of the whole data set were facilitated using the R language package *GCDkit* (Janoušek et al. 2006a).

5.1. Major and minor elements

The modal compositions of coarse-grained and inhomogeneous rocks are notoriously difficult to obtain by standard point counting techniques (e.g., Hutchison 1974). Therefore CIPW normative and not modal proportions were plotted in the QAP diagram (Streckeisen 1974) (Fig. 7a). In accord with Vrána (1989), the hyperpotassic granulites, dominated by perthitic K-feldspar, correspond mainly to alkali feldspar syenite. On the other hand, the calc-alkaline granulites span a range of compositions from gabbroic to granitic, with a frequency maximum at the felsic end of the spectrum.

The B–A diagram (Debon and Le Fort 1983; 1988) (Fig. 7b) is used to express the alumina saturation and, consequently, the characteristic mineral assemblage of igneous rocks. The hyperpotassic granulites form a trend unusual for normal magmatic compositions. The more mafic ones (higher B) are peraluminous (A > 0) but the more felsic ones straddle the boundary of the metaluminous domain (Fig. 7b, see also Tab. 8a).

The calc-alkaline granulites on the other hand range from rather mafic, falling into domains IV and V (biotite present along with other mafic phases, e.g. amphibole or pyroxene), to felsic, mica-bearing, which are slightly peraluminous (domains I–III). The majority of the calc-alkaline granulites are leucogranitic (B < 50) but for the most mafic types the parameter B exceeds 300.

The ternary diagram Na_2O – Al_2O_3 – K_2O (mol. %, Fig. 7c) shows a rather K-poor nature of the calc-alkaline granulites. On the other hand, the alkali feldspar syenitic granulites are K-rich (K_2O > 7 wt., up to 13.9; wt. % K_2O/Na_2O = 3.1–9.2 – including analyses not presented in the Tab. 8a). The literature survey revealed that there is a considerable confusion concerning the nomenclature of such rare potassium-rich rocks poor in Mg (see Mitchell and Bergman 1991 for a review). The studied *Or*-rich granulites cannot be termed *perpotassic* as this adjective is reserved for rocks, whose molar proportion of K_2O exceeds that of Al_2O_3 (Johannsen 1939; cf. Fig. 7c). They would theoretically fulfil the definitions of *ultrapotassic* igneous rocks according to some authors (Mitchell and Bergman 1991 and references therein). However, most of the authors nowadays have adopted the definition of ultrapotassic rocks after Foley et al. (1987) ($K_2O/Na_2O \geq 2$ in wt. % or 3 in mol. %, cf. Fig. 7c; each K_2O and MgO should exceed 3 wt. %). While the first two criteria are met, the studied granulites are poor in MgO (0.17–3.4 wt. %, median 0.9). Thus, in order to express the high K contents in the studied granulites and not to cause any confusion, the term '*hyperpotassic*' has been adopted here. As follows from Fig. 7c and Tab. 8a, only the sample UK5 from Lhotka is peralkaline (A/NK < 1, molar $Al_2O_3/(Na_2O + K_2O)$).

In Fig. 8 are shown Harker plots for the Blanský les granulites. The hyperpotassic types form trends largely independent of their calc-alkaline counterparts. The SiO_2 is low, below 65 % in all cases, and some rock types are rather basic (SiO_2 down to 50 %). Typical of the hyperpotassic granulites are comparably low contents most of the oxides, such as TiO_2, FeOt, MgO, CaO and Na_2O. On the other hand, enriched are K_2O (> 6.9 wt. %) and P_2O_5 (mostly >> 0.5 wt. %), as reflected by the modal abundance of K-feldspar and apatite.

The whole-rock geochemical compositions were used to obtain approximate proportions of the main rock forming minerals (wt. % – Tab. 10) by the constrained least-squares algorithm (Albarède 1995) implemented in the *GCDkit*. The assumed compositions of the rock-forming minerals were garnet UK3/A, rutile UK1/M (Tab. 3), zircon UK1/E (Tab. 4), apatite UK3/1 (Tab. 5), as well as ideal orthoclase and albite (Le Maitre 1982). The results with reasonable sums of squared residuals (R^2) would imply an overall increase, with rising silica, in K-feldspar (53 to 82 wt. %) at expense of garnet (25 to 1.5 %). The albite seems to vary rather randomly; the contents of zircon and rutile are exaggerated, as follows from the principle of the method. Given the absence of other major Zr- and Ti-bearing com-

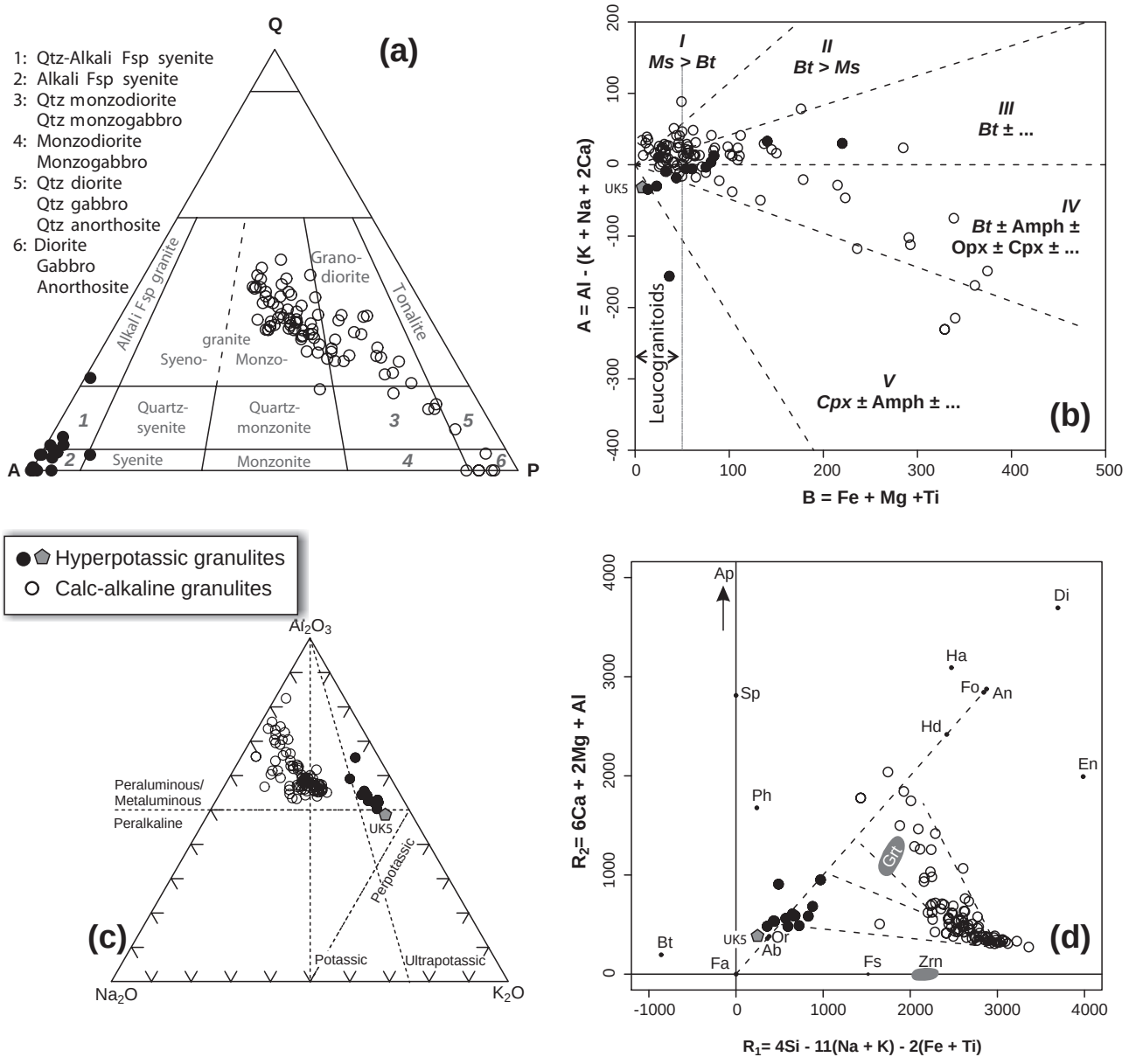

Fig. 7 Major-element based diagrams for granulites from the Blanský les Massif (for data sources, see the text). **a)** The QAP diagram (Streckeisen 1974). Instead of modal proportions, CIPW normative compositions are plotted Q = Quartz *(Qz)*, A = Alkali feldspar (*Or* + *Ab* for perpotassic and *Or* for calc-alkaline granulites), P = Plagioclase (*An* for perpotassic and *Ab* +*An* for calc-alkaline granulites). **b)** Multicationic plot B–A (B being proportional to the amount of mafic minerals and A expressing the alumina saturation) (Debon and Le Fort 1983; 1988). **c)** Ternary plot Na_2O – Al_2O_3 – K_2O (mol. %). Dashed lines define the following compositional fields: peraluminous + metaluminous, $(Na_2O+K_2O)/Al_2O_3 < 1$; peralkaline, $(Na_2O+K_2O)/Al_2O_3 > 1$; perpotassic, $K_2O/Al_2O_3 > 1$ and $K_2O/Na_2O > 1$; potassic, $1 < K_2O/Na_2O < 3$; and ultrapotassic, $K_2O/Na_2O \geq 3$ in mol. % (or $K_2O/Na_2O \geq 2$ in wt. %, which is equivalent to the definition of ultrapotassic igneous rocks by Foley et al. 1987). **d)** Modification of the R_1–R_2 diagram (De La Roche et al. 1980) according to Batchelor and Bowden (1985). Plotted are also ideal mineral compositions of the main rock-forming minerals (Le Maitre 1982) as well as compositional fields for garnet (Grt) and zircon (Zrn) from the studied samples. Apatite (Ap) with $R_2 \sim 5900$ is out of the limits.

ponents, better seem to be theoretical upper limits provided by the calculated wt. % of $ZrSiO_4$ and TiO_2 (Tab. 10). The estimated zircon contents then would seem to drop sharply from *c.* 0.77 wt. % for the mafic types (sample BD158) to 0.01 % in the felsic lithologies as do the rutile contents (from *c.* 0.3 to 0.03 wt. %).

5.2. Trace elements

The trace-element evolution of the hyperpotassic granulites is shown in the form of binary plots with SiO_2 on abscissa (Fig. 9). There is a marked tendency to an increase in LILE contents (Rb, Sr, Ba) accompanied by a sharp

Tab. 9a Trace-element whole-rock chemical composition of the potassic granulites from the Blanský les Massif (ppm)

	BD158	BD159	BD160b	LV122	Fi20/02a	Fi20/02b	Fi21/02	Fi22/02	UK2	UK3	UK5
Laboratory*	SBG, INAA	SBG, INAA	SBG, INAA	SBG, INAA	SBG	SBG	SBG	SBG	ACME	ACME	ACME
Rb	570	557	542	644	543	499	591	605	476	593	332
Cs	13.2	9.2	9.6	9.0	12.5	12.7	9.7	9.9	10.9	12.6	5.2
Sr	304	131	185	233	230	204	245	259	229	288	381
Ba	1044	706	979	1083	1254	1164	1328	1589	1133	1361	6310
Nb	12	11	7	2	12	17	2	2	1	<0.5	<0.5
Ta	–	–	–	–	–	–	–	–	<0.1	<0.1	<0.1
Zr	3812	279	73	510	754	1177	53	5	1373	3048	1
Hf	155	11	2	18	23	37	1	b.d.	36.1	78.0	<0.5
Ga	11	13	13	17	17	17	15	17	15.5	16.7	15.7
Th	*31*	*9*	*7*	*4*	–	–	–	–	7.2	6.1	3.5
U	*9.7*	*2.9*	*<0.6*	*<0.7*	–	–	–	–	4.6	7.1	0.7
Cr	22	37	29	15	27	38	12	44	13.7	6.8	6.8
Ni	25	17	9	13	17	23	8	40	17	5	13
Co	6	12	8	5	5	6	2	4	4.5	2.2	0.6
V	8	26	13	2	18	19	6	35	12	6	<5
Sc	6	16	8	1	7	11	2	1	7	1	1
Pb	24	11	15	19	21	21	22	21	1.1	1.5	7.0
Cu	71	10	6	15	3	5	1	2	1.4	1.1	1.9
Zn	27	67	38	13	31	38	15	37	28	12	1
La	*345.4*	*87.5*	*80.2*	*75.0*	–	–	–	–	80.7	66.5	27.9
Ce	*849.8*	*177.3*	*156.3*	*132.5*	–	–	–	–	178.1	142.9	57.6
Pr	–	–	–	–	–	–	–	–	19.49	14.77	6.17
Nd	*411*	*91*	*85*	*64*	–	–	–	–	70.4	52.6	23.0
Sm	*60.7*	*18.3*	*16.6*	*12.5*	–	–	–	–	13.8	10.4	4.4
Eu	*5.50*	*1.69*	*1.45*	*1.41*	–	–	–	–	1.72	1.50	0.72
Gd	–	–	–	–	–	–	–	–	11.16	7.75	3.07
Tb	*9.8*	*3.6*	*2.9*	*1.4*	–	–	–	–	2.04	1.35	0.41
Dy	–	–	–	–	–	–	–	–	12.59	7.65	1.92
Ho	–	–	–	–	–	–	–	–	2.48	1.46	0.29
Er	–	–	–	–	–	–	–	–	7.11	3.80	0.63
Tm	–	–	–	–	–	–	–	–	1.19	0.54	0.07
Yb	*10.2*	*14.6*	*9.6*	*1.5*	–	–	–	–	7.24	3.52	0.51
Lu	*1.03*	*1.72*	*1.18*	*0.15*	–	–	–	–	1.03	0.44	0.05
Y	225	89	65	43	71	93	29	32	76	45	9
Eu/Eu*	–	–	–	–	–	–	–	–	0.4	0.5	0.6
La_N/Yb_N	22.8	4.0	5.6	33.7	–	–	–	–	7.5	12.7	36.9
La_N/Sm_N	3.6	3.0	3.0	3.8	–	–	–	–	3.7	4.0	4.0
ΣREE	–	–	–	–	–	–	–	–	409.0	315.2	126.7
K/Rb	177.7	129.1	167.7	179.0	176.6	178.2	186.8	181.0	194.1	171.3	369.8
Rb/Sr	1.9	4.3	2.9	2.8	2.4	2.4	2.4	2.3	2.1	2.1	0.9
Rb/Cs	43.8	61.9	54.2	71.6	41.8	38.4	59.1	60.5	43.7	47.1	63.8

* Laboratories: **SBG:** XRF, pressed pellets, Division of Mineralogy and Material Science, University of Salzburg, Austria;
INAA: Instrumental Neutron Activation Analysis, laboratories of Geoindustria Inc., Prague-Černošice (italics);
ACME: mostly ICP-MS, Acme Analytical Laboratories Ltd., Vancouver, Canada.

'b.d.' and values 'less than': below detection limit, '–': not determined

drop in Y, together with some elements generally hosted by mafic phases (i.e. garnet; Zn and Sc). The decrease in La and Eu is much less obvious.

The chondrite-normalized (Boynton 1984) REE patterns for the garnet-bearing samples (Fig. 10a) vary a little in their LREE segments (La_N = 215–285 × chondrite) except

Tab. 9b Trace–element whole–rock chemical composition of the calc–alkaline granulites from the Blanský les Massif (ppm)

	BD160a	1060	1061	1063	1065	1066	1067	1068	1069	1070
Laboratory*	SBG, INAA	SBG, CGS	SBG, CGS	SBG, CGS	SBG, CGS	SBG, CGS	SBG, CGS	SBG, CGS	SBG, CGS	SBG, CGS
Rb	313	98	118	103	119	54	51	72	88	158
Cs	4.9	2.6	4.8	3.3	4.1	4.6	4.8	4.0	3.9	3.4
Sr	50	149	80	39	53	87	78	120	54	54
Ba	142	1074	819	217	281	470	373	987	128	142
Nb	3	6	7	3	2	5	14	9	3	3
Zr	20	162	158	26	27	86	182	213	34	21
Hf	1	5	5	1	1	2	6	7	1	1
Ga	17	17	18	17	17	20	24	20	19	18
Th	1	4	8	0	2	2	2	21	0	0
U	<0.5	3	3	3	3	3	b.d.	4	4	4
Sc	5	7	6	4	4	8	19	12	5	4
Pb	6	12	3	3	7	4	3	5	2	1
Cu	5	5	8	3	3	7	18	15	b.d.	b.d.
Zn	22	38	37	27	16	40	84	59	23	21
La	12.4	30.4	24.7	8.7	9.7	15.8	24.4	40.6	15.5	11.3
Ce	18.6	64.9	63.5	22.0	19.1	48.0	61.6	96.2	38.7	27.1
Pr	–	8.02	8.79	3.32	1.61	6.21	8.09	13.97	5.11	2.52
Nd	11.0	29.8	33.2	11.2	8.5	25.5	33.9	49.7	19.6	13.4
Sm	2.92	5.85	6.70	2.42	1.95	5.71	8.18	9.93	4.35	3.01
Eu	0.23	0.82	0.76	0.22	0.17	0.95	1.31	1.33	0.45	0.29
Gd	–	5.80	6.42	3.13	2.26	6.51	9.11	9.47	4.79	3.26
Tb	0.60	0.88	1.34	0.75	b.d.	1.86	1.84	1.58	0.90	0.00
Dy	–	5.68	6.84	4.63	3.36	7.68	8.31	7.89	5.60	4.77
Ho	–	1.21	1.43	0.99	0.76	1.49	1.56	1.47	1.16	1.00
Er	–	3.56	4.26	3.51	2.28	4.76	4.64	4.11	3.35	2.99
Tm	–	0.39	0.42	0.42	0.32	0.56	0.44	0.54	0.39	0.33
Yb	2.50	3.40	3.75	3.31	1.90	4.13	4.03	3.92	2.95	2.58
Lu	0.32	0.49	0.55	0.50	0.27	0.61	0.62	0.58	0.41	0.34
Y	23	33	40	27	20	48	47	45	32	27
Eu/Eu*	–	0.4	0.4	0.2	0.2	0.5	0.5	0.4	0.3	0.3
La_N/Yb_N	3.3	6.0	4.4	1.8	3.4	2.6	4.1	7.0	3.5	2.9
La_N/Sm_N	2.7	3.3	2.3	2.3	3.1	1.7	1.9	2.6	2.2	2.4
ΣREE	48.6	161.2	162.6	65.1	52.2	129.8	168	241.2	103.2	72.8
K/Rb	138.2	328.7	280.7	293.4	284.6	335.1	250.7	352.8	202.8	176.5
Rb/Sr	6.3	0.7	1.5	2.6	2.2	0.6	0.7	0.6	1.6	2.9
Rb/Cs	63.9	37.7	24.6	31.2	29.0	11.7	10.6	18.0	22.6	46.5

* Laboratories: **SBG:** XRF on pressed pellets, Division of Mineralogy and Material Science, University of Salzburg, Austria; **CGS:** REE determined by ICP-ES, Czech Geological Survey, Prague.

for the mafic granulite BD158 (La_N > 1100). All are characterised by pronounced negative Eu anomalies (Eu/Eu* = 0.42–0.51). A peculiar feature is the great range in HREE contents, which drop sharply with rising silica (e.g., Yb_N from 70 to 7 × chondrite). As a consequence, the degree of LREE/HREE fractionation is also variable and rising (La_N/Yb_N = 4–37). The Lhotka sample UK5 shows the lowest total REE contents (ΣREE = 127), being strongly depleted in both LREE and HREE (La_N = 90, Yb_N = 2.4; i.e. La_N/Yb_N = 37) but showing a less significant Eu anomaly (Eu/Eu* = 0.60).

Average upper crust normalized spider plots (Taylor and McLennan 1995) are characterised by conspicuous troughs in some HFSE (Nb and Ti; Ta being always below its detection limit of 0.1 ppm; Fig. 10b). Typical of the garnet-bearing samples are variable but usually high concentrations of Zr and Hf, accompanied by enrichment in LILE (Cs, Rb, Ba, U and K) as well as P and REE + Y. Thorium is variably depleted. On the other hand, the sample UK5 contains relatively low Zr, Hf, U, Th and REE (especially HREE) concentrations; its Ba is higher still.

1071	1072	1075	1077	1079	1080
SBG, CGS	SBG, CGS	SBG, CGS	SBG, CGS	SBG, CGS	SBG, CGS
185	185	179	147	75	128
4.3	3.9	5.4	4.3	3.8	4.6
33	78	60	90	83	106
93	442	266	568	231	680
3	7	6	7	15	7
b.d.	105	86	103	110	137
b.d.	3	3	3	4	3
18	18	20	18	21	19
b.d.	b.d.	1	1	b.d.	2
3	1	2	2	1	b.d.
4	5	4	6	11	7
1	7	5	4	3	2
2	2	5	8	20	15
43	38	38	40	76	48
4.9	19.6	19.1	8.0	15.7	20.0
12.5	45.3	42.9	32.9	36.4	44.0
1.52	5.73	5.41	3.59	5.07	4.38
5.6	23.3	20.5	20.8	20.3	20.2
1.31	4.62	5.17	4.85	4.69	4.17
0.16	0.69	0.54	0.76	0.96	0.62
1.43	5.57	5.13	5.91	5.95	4.10
0.00	0.89	0.90	0.97	0.73	0.88
3.17	7.13	7.34	7.29	5.96	4.70
0.62	1.61	1.47	1.66	1.11	0.90
1.87	4.63	4.88	4.56	3.69	2.73
0.27	0.64	0.46	0.54	0.35	0.38
2.45	4.25	4.39	4.27	3.20	2.97
0.33	0.58	0.61	0.58	0.44	0.45
19	44	45	45	37	51
0.4	0.4	0.3	0.4	0.6	0.5
1.4	3.1	2.9	1.3	3.3	4.5
2.4	2.7	2.3	1	2.1	3
36.1	124.6	118.8	96.7	104.6	110.5
137.3	206.0	198.0	244.0	257.9	269.8
5.6	2.4	3	1.6	0.9	1.2
43.0	47.4	33.1	34.2	19.7	27.8

'b.d.' and values 'less than': below detection limit,
'–': not determined

The hyperpotassic granulites show many important differences compared to the calc-alkaline types. These are highlighted in ‚spider percentile boxplots' normalised by an average composition of the BLGM calc-alkaline granulites (Fig. 10c, see the figure caption for explanation). The most striking is 2–5× enrichment in lithophile elements, especially those which are feldspar-compatible. Characteristic are elevated contents of Cs, Rb, Ba, U, K, Sr and Pb. The hyperpotassic granulites are also enriched in P, Zr, Hf and REE (in LREE + MREE more than in HREE + Y). Contents some of the HFSE, such as Th and Ga, are comparable to the average of the calc-alkaline granulites. On the other hand, the Nb shows a considerable range (being mostly variably depleted); the Ti concentrations are consistently very low.

5.3. Apatite and zircon saturation temperatures

Saturation temperatures for the main accessories (apatite, zircon and monazite) have been calculated in order to constrain the liquidus temperature of the magma parental to the hyperpotassic granulites (see Janoušek 2006 for discussion of the calculation algorithms used). They should be applicable given the presence of early, large euhedral crystals of apatite and zircon, as well as the (rough) negative correlations of P, Zr and LREE with the increasing silica. The apatite saturation temperatures (Harrison and Watson 1984) are comparable for all garnet-bearing samples, averaging to 1070 ± 150 °C (median ± 2σ) (Fig. 11). However, the zircon saturation temperatures (Watson and Harrison 1983) for garnet-bearing granulites span a wide range between *c.* 1150 and 550 °C. The pyroxene-bearing sample UK5 yields even lower value of 460 °C (Fig. 11). The monazite saturation temperatures (Montel 1993) are surprisingly low, 833 and 810 °C for samples UK2 and UK3, 723 °C for UK5. This might be linked to the extreme scarcity of primary monazite and the fact that much of the LREE seems to have entered initially another phase (apatite). If true, this would render the calculated monazite saturation temperatures meaningless.

5.4. Sr–Nd isotopes

Newly obtained whole-rock Sr–Nd isotopic ratios for the hyperpotassic granulites, age-corrected to 337 Ma, are presented in the Tab. 11 and Fig. 12. One of the samples is of the Lhotka type (UK5) and two are typical garnet-bearing hyperpotassic granulites (Plešovice type, UK2 and UK3).

The Nd isotopic compositions do not vary greatly for the three ($\varepsilon_{Nd}^{337} \sim -5.5$), corresponding to uniform two-stage Nd depleted-mantle model ages (T_{Nd}^{DM} = 1.47–1.49 Ga). There are, however, more pronounced differences in the Sr isotopic compositions (Fig. 12b). The signatures of the two Plešovice granulites are mutually comparable ($^{87}Sr/^{86}Sr_{337}$ = 0.7272 and 0.7279) but significantly more radiogenic than for the Lhotka sample UK5 ($^{87}Sr/^{86}Sr_{337}$ = 0.7109). The $^{87}Sr/^{86}Sr_{337} - \varepsilon_{Nd}^{337}$ plot (Fig. 12) shows clearly that the Sr–Nd isotopic compositions of the hyperpotassic granulites fall within the compositional range of the calc-alkaline granulites but far from typical Moldanubian lower grade metasediments.

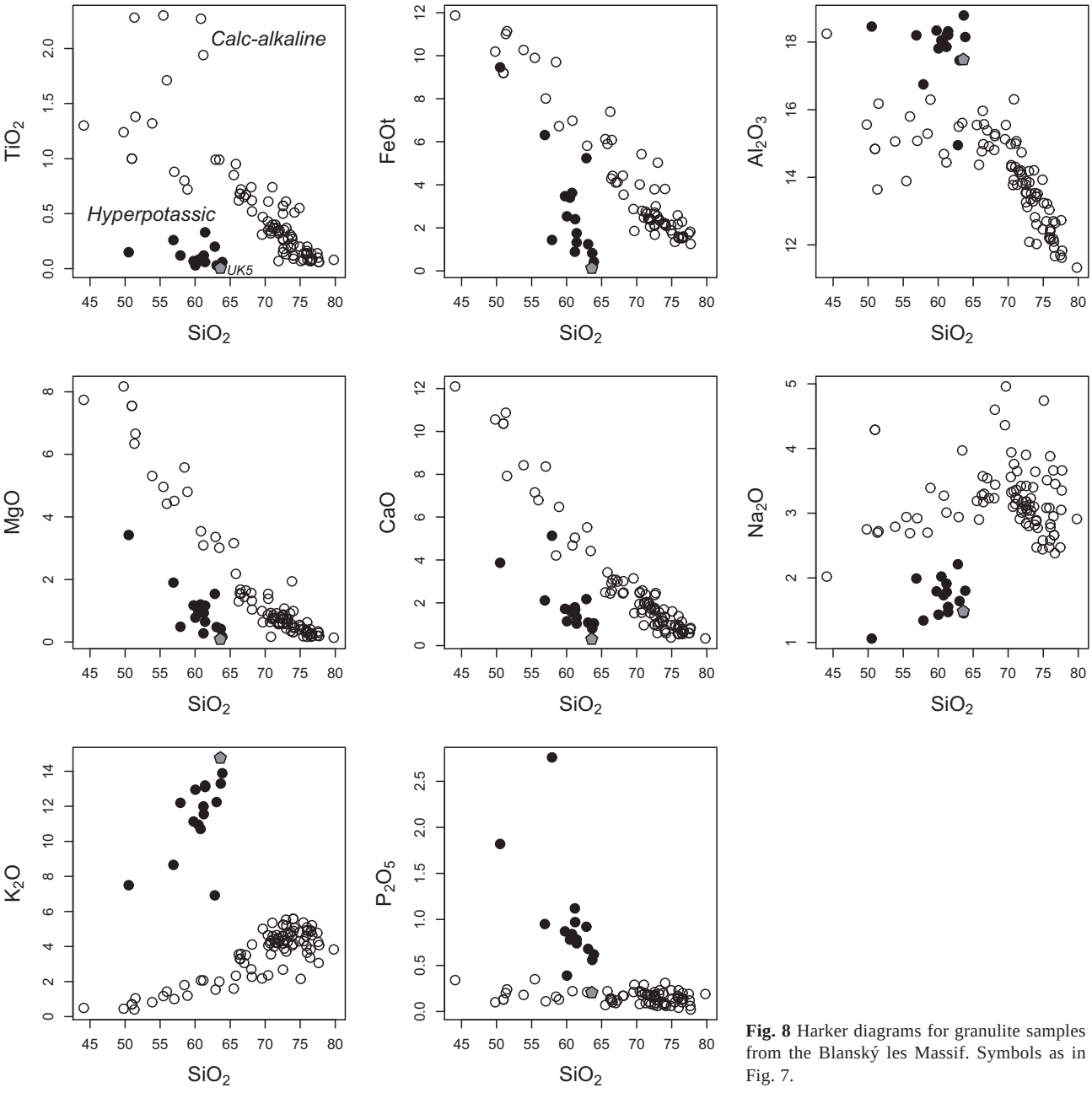

Fig. 8 Harker diagrams for granulite samples from the Blanský les Massif. Symbols as in Fig. 7.

6. Discussion

6.1. Are the hyperpotassic granulites igneous or metamorphic rocks?

The idea that the hyperpotassic granulites represent Variscan (*c.* 337 Ma) melts and not metamorphic rocks, championed already by Vrána (1989), is confirmed by several lines of evidence. If metamorphic, an unusual protolith would be required with an extraordinary geochemical signature. Moreover, enclosed in K-feldspar is a number of large euhedral zircon crystals devoid of any pre-Viséan inherited component. These all show oscillatory zoning and are thus hard to explain by metamorphic recrystallization. The argument is strengthened by the presence of euhedral zircon crystals enclosed in garnet, suggestive of heterogeneous nucleation on the growing crystal faces of their garnet host.

6.2. Significance of the zircon, apatite and monazite saturation temperatures

The apatite saturation temperatures obtained for the Grt-bearing hyperpotassic granulites (*c.* 1050 °C) are relatively constant and close to the previous peak tem-

Tab. 10 Estimated mineral proportions (wt. %, least-squares method)

	LV122	estim.	diff.	BD160b	estim.	diff.	BD159	estim.	diff.
SiO_2	63.87	63.84	0.03	60.46	60.45	0.01	56.89	56.97	-0.08
Al_2O_3	18.15	18.22	-0.07	18.05	18.55	-0.50	18.20	18.85	-0.65
FeOt	0.42	0.39	0.03	3.40	3.42	-0.02	6.32	6.45	-0.14
MnO	0.00	0.01	-0.01	0.07	0.10	-0.03	0.11	0.19	-0.08
MgO	0.17	0.11	0.07	0.99	0.92	0.07	1.90	1.73	0.17
CaO	1.04	0.96	0.08	1.66	1.77	-0.11	2.11	2.45	-0.34
Na_2O	1.80	1.76	0.04	2.02	2.20	-0.18	1.99	2.26	-0.27
K_2O	13.89	13.86	0.03	10.95	11.11	-0.16	8.66	8.91	-0.25
ZrO_2	0.06	0.06	0.00	0.01	0.18	-0.17	0.04	0.32	-0.29
TiO_2	0.06	0.05	0.01	0.08	0.19	-0.11	0.26	0.47	-0.21
P_2O_5	0.62	0.69	-0.07	0.78	0.90	-0.12	0.95	1.01	-0.06
		R^2 =	0.024		R^2 =	0.376		R^2 =	0.863

	wt. %
Or	81.9
Ab	14.8
Grt	1.5
Ap	1.6
Zrn	0.1
Rt	0.0

	wt. %
Or	65.6
Ab	18.6
Grt	13.2
Ap	2.1
Zrn	0.3
Rt	0.2

	wt. %
Or	52.7
Ab	19.1
Grt	24.9
Ap	2.4
Zrn	0.5
Rt	0.5

Sample	Or	Ab	Grt	Zrn	Ap	Rt	R^2	$ZrSiO_4$	TiO_2
Fi20/02a	71.4	20.0	4.1	0.6	3.4	0.5	3.2	0.15	0.12
Fi20/02b	67.8	22.1	5.0	1.0	3.4	0.6	5.4	0.24	0.09
Fi21/02	80.5	15.9	2.0	0.1	1.5	0.1	1.0	0.01	–
Fi22/02	79.2	13.3	3.9	0.4	2.5	0.7	3.0	0.00	0.33
BD158	72.6	12.0	6.1	0.9	8.2	0.2	0.7	0.77	0.12
BD159	52.7	19.1	24.9	0.5	2.4	0.5	0.9	0.06	0.26
BD160b	65.6	18.6	13.2	0.3	2.1	0.2	0.4	0.01	0.08
LV122	81.9	14.8	1.5	0.1	1.6	0.0	0.0	0.10	0.06
UK2	66.8	16.5	13.7	0.5	2.3	0.2	0.5	0.28	0.07
UK3	74.5	18.3	4.4	0.9	1.7	0.1	1.1	0.61	0.03
1	71.4	20.0	4.1	0.6	3.4	0.5	3.2	1.18	0.07
2	67.8	22.1	5.0	1.0	3.4	0.6	5.4	0.24	0.15
2a	77.4	12.4	7.6	0.2	2.2	0.2	0.2	0.00	0.06

perature estimates for both the hyperpotassic garnet-bearing (Vrána 1989) and great many of the Moldanubian calc-alkaline granulites (see O'Brien and Rötzler 2003; Janoušek et al. 2006b for reviews). On this basis they can be taken as reasonable estimates of the magma's liquidus temperature.

The discrepancy between consistently high apatite and extremely variable, but mostly lower, zircon saturation temperatures (Fig. 11) is difficult to explain. The variations in the M parameter (cationic ratio $\frac{Na+K+2Ca}{Al.Si}$) – on which the zircon solubility depends the most decisively (Watson and Harrison 1983) – are small and thus cannot be the primary cause. Nevertheless, there seem to be several additional factors controlling the zircon solubility, such as the abundances of fluorine (Keppler 1993) and iron (Baker et al. 2002). Thus some of the variation may be due to local fluctuations in the chemistry of the parental magma.

In addition, the irregular distribution of the zircon in the hyperpotassic granulites requires very large sample sizes for the whole-rock chemical analyses to be truly representative. It may not be incidental that the two newly collected, particularly large samples (UK2 and UK3)

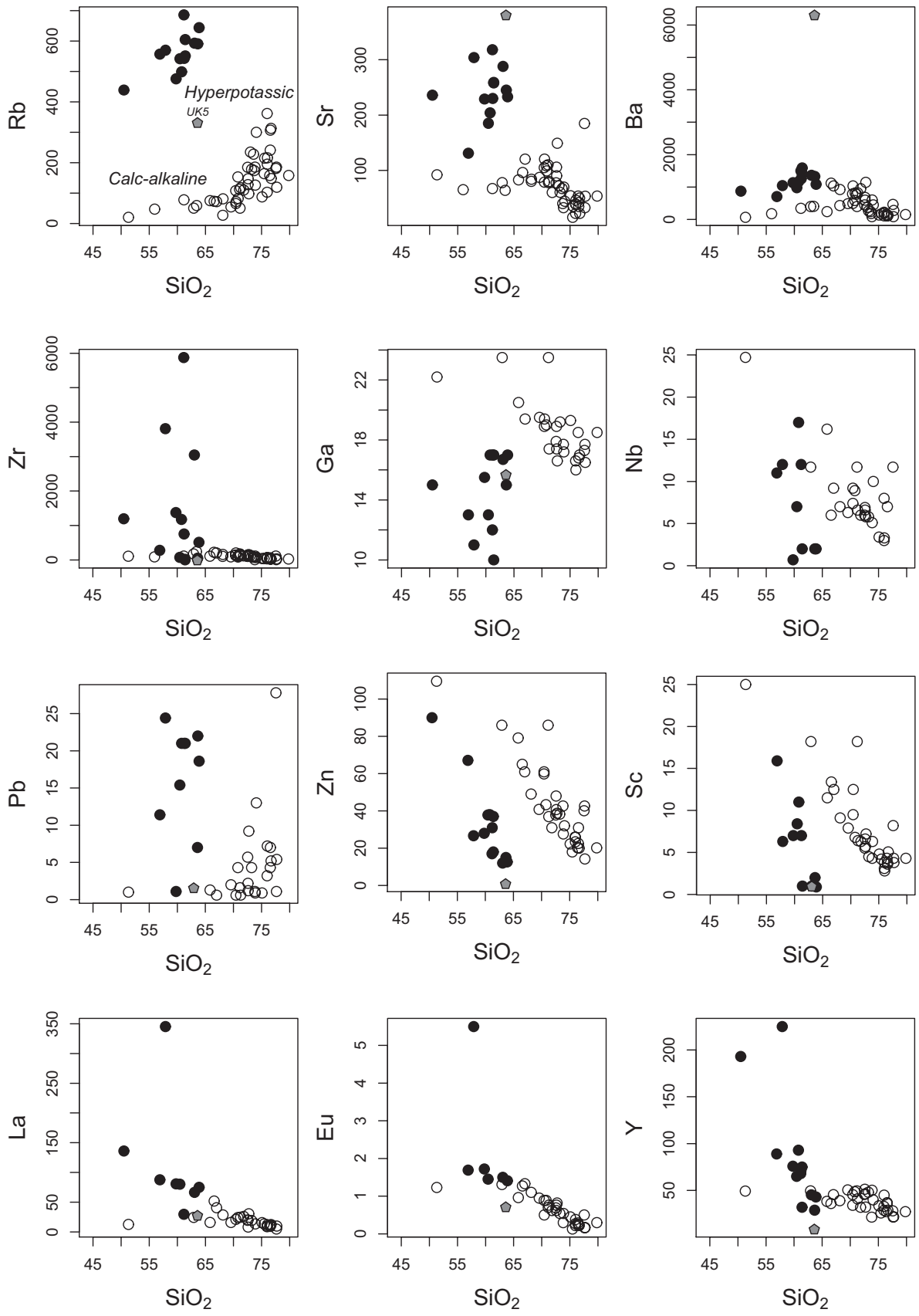

Fig. 9 Binary diagrams of SiO_2 versus selected trace elements (ppm). Symbols as in Fig. 7.

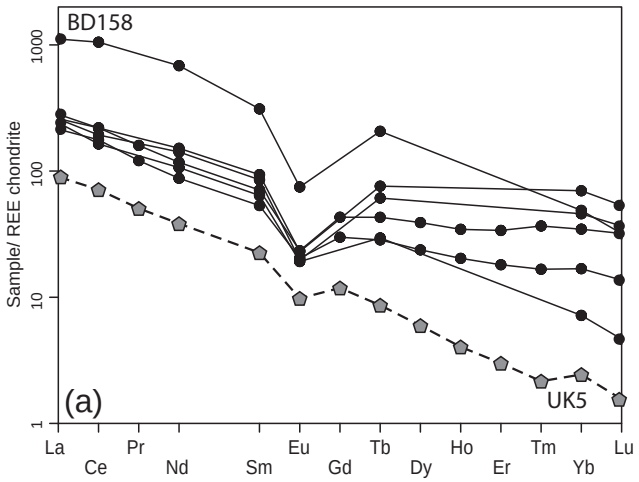

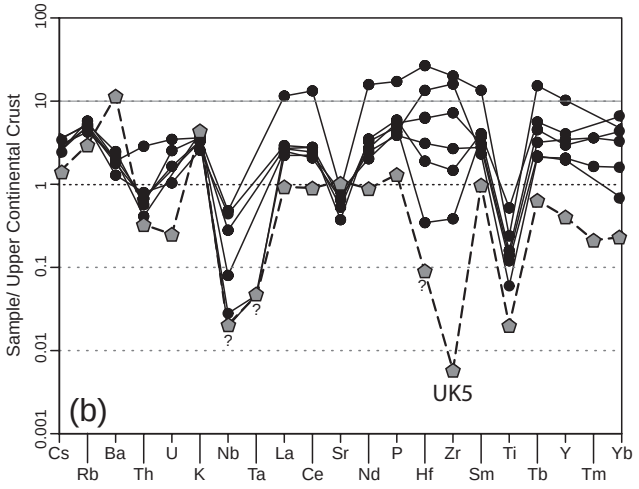

Normalized by an average of CA granulites from BLGM

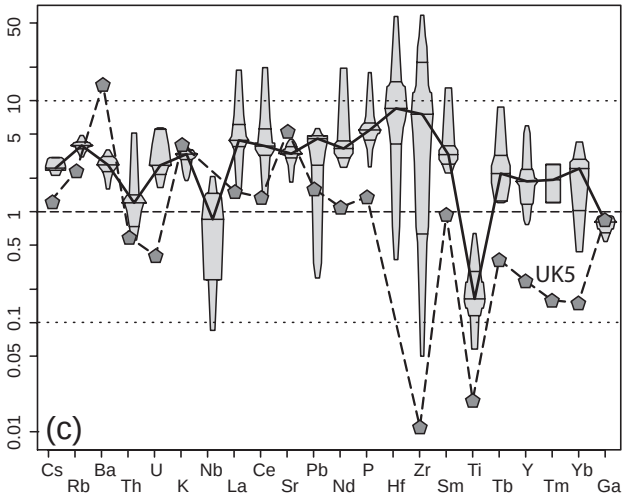

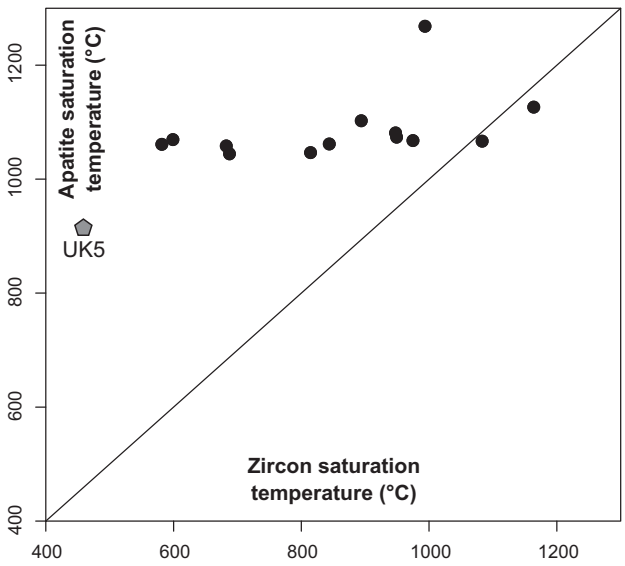

Fig. 11 Binary plot of apatite vs. zircon saturation temperatures. The temperatures for apatite have been calculated using the saturation model of Harrison and Watson (1984); those for zircon following Watson and Harrison (1983).

yield reasonable zircon saturation temperatures (975 and 1083 °C). The rather large zircon crystals could have been settling and accumulating in some domains of the intruding and crystallizing magma. Clearly, some of the samples may not reflect the true melt composition at all, representing instead Zr-depleted, feldspar-rich cumulates (e.g., UK5 with 1 ppm of Zr).

Finally, given the high Zr saturation levels required by the hot, alkali-rich magmas parental to the hyperpotassic granulites, kinetic factors could have played a major role. There may be problems with attaining equilibrium during dry, rather short-lived anatectic events when the Zr, P and LREE diffusion is sluggish (Harrison and Watson 1983; Harrison and Watson 1984; Watson and Harrison 1984; Rapp and Watson 1986; Watson 1996). The heterogeneity of the source, coupled with small equilibration distances in relatively dry systems and a possibility of isolation of

⇐

Fig. 10 a) Chondrite-normalized (Boynton 1984) REE patterns for the hyperpotassic granulites. **b)** Average upper crust normalized (Taylor and McLennan 1995) spider plots for hyperpotassic granulites from the Blanský les granulite Massif. Question marks indicate values that were below the limit of detection (and thus should be taken as an upper constraint). **c)** 'Spider box and percentile plot' for hyperpotassic granulites, normalized by an average of the calc-alkaline felsic granulites from the Blanský les granulite Massif. In this diagram, based on Esty and Banfield (2003), the distribution of each of the normalized trace-element contents is plotted as irregular polygons. Their width at any given height is proportional to the empirical cumulative distribution. As in boxplots, the median, 25th, and 75th percentiles are marked with horizontal line segments across the box.

Tab. 11 Sr–Nd isotopic data for hyperpotassic granulites from the Blanský les granulite Massif

Sample	Rb (ppm)	Sr (ppm)	$^{87}Rb/^{86}Sr$	$^{87}Sr/^{86}Sr$	2 s.e.	$(^{87}Sr/^{86}Sr)_i$	Sm (ppm)	Nd (ppm)	$^{147}Sm/^{144}Nd$
Garnet-bearing hyperpotassic granulites, Plešovice quarry									
UK2	476.2	228.8	6.0506	0.756234	12	0.727210	13.8	70.4	0.1185
UK3	593.0	288.4	5.9778	0.756527	12	0.727853	10.4	52.6	0.1195
Pyroxene-bearing hyperpotassic granulite, Lhotka									
UK5	331.5	381.2	2.5199	0.722980	12	0.710893	4.4	23.0	0.1156

Sample	$^{143}Nd/^{144}Nd$	2 s.e.	$(^{143}Nd/^{144}Nd)_i$	ε^i_{Nd}	T^{CHUR}_{Nd} (Ga)	T^{DM}_{Nd} (Ga)
Garnet-bearing hyperpotassic granulites, Plešovice quarry						
UK2	0.512191	18	0.511929	-5.4	0.87	1.47
UK3	0.512180	8	0.511916	-5.6	0.91	1.49
Pyroxene-bearing hyperpotassic granulite, Lhotka						
UK5	0.512178	9	0.511923	-5.5	0.87	1.48

Isotopic ratios with subscript 'i' were all age-corrected to 337 Ma (Aftalion et al. 1989; Sláma et al. 2006).
(T^{DM}_{Nd}) = two-stage Nd model ages calculated after Liew and Hofmann (1988).

the zircon grains in the refractory phases, especially at small melting rates (Harrison & Watson 1983; Watson 1996), may have resulted in production of variably Zr-undersaturated magma batches.

6.3. Relationship between the two types of the hyperpotassic granulites

The (limited) isotopic data presented in the current paper demonstrate that the sources yielding the two types of hyperpotassic granulites (garnet- and pyroxene bearing) were homogeneous in respect to their Sm–Nd isotopic composition and thus also the mean crustal residence age. Even though both samples UK3 and UK5 share a similar modal composition (both being for instance rich in K-feldspar) and also resemble each other in terms of the whole-rock major-element chemistry, they differ markedly in a wide range of trace elements (Fig. 10c). The fact that sample UK5 crystallized pyroxene and not garnet is probably due to its too low A/CNK and A/NK values, coupled with low whole-rock Fe and Ca contents. In addition, the concentration of Ca could have been further lowered by the early growth of apatite.

The extremely high whole-rock Ba value of ~6 400 ppm in the sample UK5 supports its cumulate origin. Given the very high $D(Ba)^{Fsp/granitic\ liquid}$ of 0.07 + 0.25 × *(mol. % orthoclase)* as derived from experiments of Icenhower and London (1996), the parental melt should have contained some 300–500 ppm Ba.

The low Zr content in UK5 not only explains the absence of zircon but also shows that the Zr–Ti rich inclusions in broken down pyroxene must be secondary, otherwise, when primary, their extremely high Zr values would require a saturation in Zr. The situation resembles the REE-enriched Ti phase. As early-grown apatite (and probably some monazite) would represent a profound REE sink, there should be no reason for such a REE-rich Ti phase to form during the primary crystallization. Thus, it is more likely that these REE–Ti-rich phases emerged secondary, for instance, from originally alkali-rich (Al, Ti rich) pyroxenes, which have a higher affinity to REE + Y (Hack et al. 1994) and HFSE (Gallahan and Nielsen 1992; Forsythe et al. 1994).

A crucial point is that the two types of hyperpotassic granulites differ markedly in their Sr isotopic compositions. Thus the pyroxene-bearing Lhotka granulites could not have been derived by closed-system fractional crystallization/accumulation from their more common, garnet-bearing counterparts occurring in the Plešovice quarry. This is to be expected given the geographic distance between the two occurrences, together with paucity and small size of the known hyperpotassic granulite bodies. The easiest explanation for generation of the magmas parental to the two types is remelting of the same, pre-existing crustal segment with a rather constant, time-integrated Sm/Nd ratio. The regional differences in Rb/Sr ratios of this pre-Variscan protolith and consequently variable *in situ* growth of the radiogenic Sr with time could account for the dichotomy in the $^{87}Sr/^{86}Sr$ ratios.

6.4. Constraints on the possible source

Available analyses of the Czech Moldanubian metasediments (paragneisses and melt-depleted, garnet-bearing residua after HT anatexis) have epsilon Nd values significantly lower and Sr isotopic signature mostly less

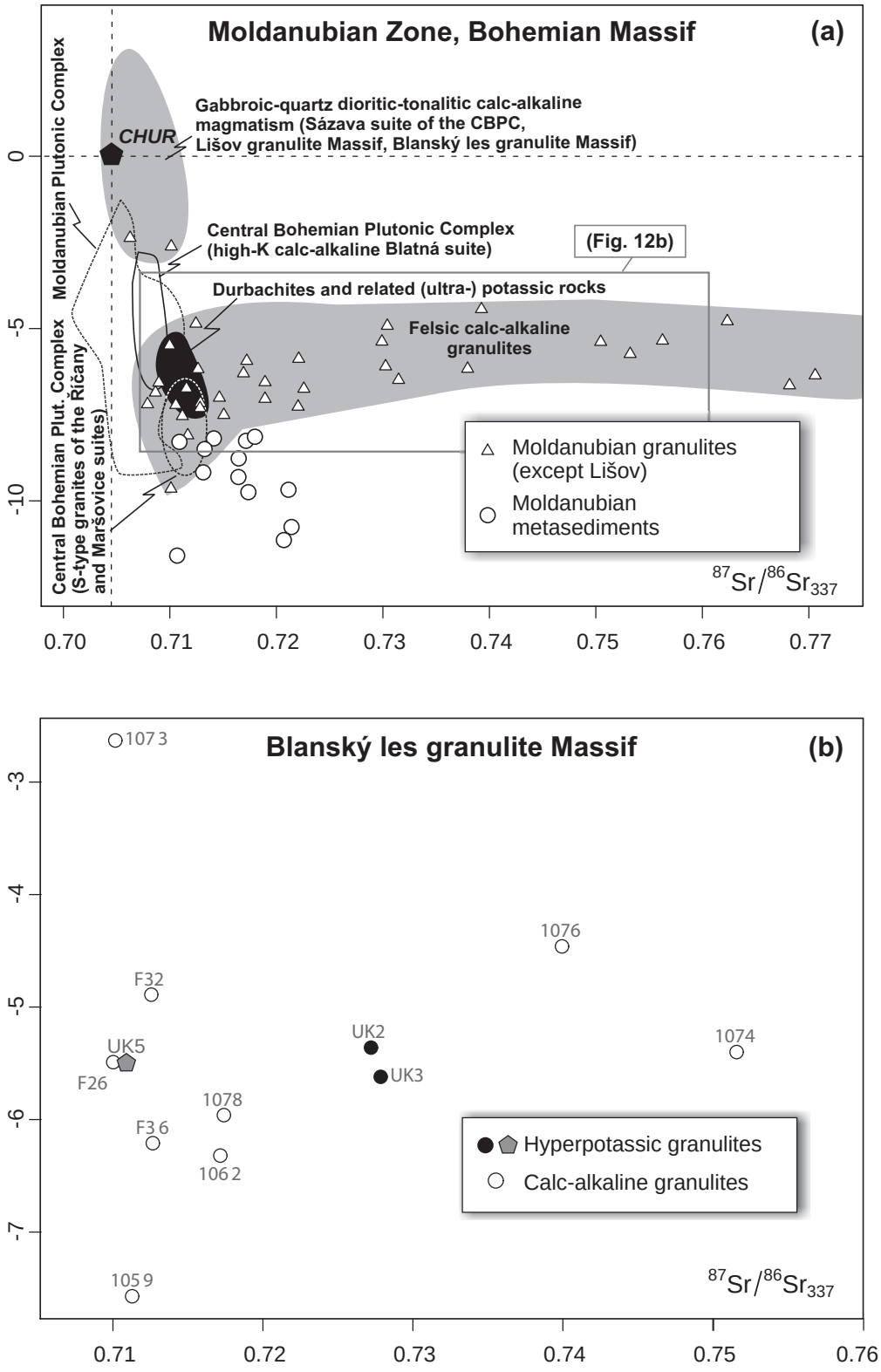

Fig. 12 a) Diagram $^{87}Sr/^{86}Sr_{337}$ vs. ε_{Nd}^{337} for selected rock types from the Moldanubian Zone of the Bohemian Massif: granitoids of the Moldanubian Plutonic Complex (Liew et al. 1989; Vellmer and Wedepohl 1994; Gerdes 1997; Janoušek et al. 2002), granitoids of the Central Bohemian Plutonic Complex (CBPC: Janoušek et al. 1995; Sokol et al., 2000), durbachitic rocks (Holub and Janoušek 2003), Moldanubian metasediments (Janoušek et al. 1995 and unpublished data) as well as Moldanubian calc-alkaline granulites (Vellmer 1992; Valbracht et al. 1994; Becker et al. 1999; Janoušek et al. 2004; 2006b). **b)** Detail of an analogous plot involving solely the granulites from the Blanský les granulite Massif both calc-alkaline (Valbracht et al. 1994; Janoušek et al. 2004) and hyperpotassic (this work).

radiogenic than the hyperpotassic granulites described in the present work (Fig. 12a). On this basis an origin by partial melting of metasedimentary rocks, similar to those cropping out in the Moldanubian Unit, is considered unlikely.

On the other hand, the hyperpotassic granulites show enrichments complementary to the depletions observed in the spatially and temporally associated felsic calc-alkaline granulites (e.g., Cs, Rb, U, Zr and Hf); moreover, both granulite groups share a matching Sr–Nd isotopic signature. The temperature estimates for the hyperpotassic granulites and peak of the high-grade metamorphism in South Bohemian granulite massifs are also grossly comparable (Vrána 1989; Owen and Dostal 1996; Svojtka et al. 2002). Finally, the intrusion age for the hyperpotassic granulites is close to, if not slightly younger than, the best age estimates for this HP–HT metamorphic climax.

Therefore there is a viable possibility that the hyperpotassic granulites represent rare, low-scale melts that managed to separate and escape from the common granulitic lithologies of the BLGM. This would have to have taken place at the granulite-facies metamorphic peak or in early stages of the uplift.

6.5. Role for Variscan HP melting?

The great many of the CIPW-normative compositions of the felsic Moldanubian granulites (SiO_2 > 70 wt. %) fall close to the low-pressure, (nearly) H_2O-saturated minimum in the Ab–Qz–Or ternary (Fig. 13; see also Fiala et al. 1987a; Vrána 1989). This demonstrates that they represent magma compositions with little cumulate or restite component. However, for most of the samples, no significant shift to Qz–Or join envisaged by Kotková and Harley (1999) could have been confirmed. On the contrary, the position of the frequency maximum in the Ab–Qz–Or ternary seems to argue rather for a low-pressure, essentially eutectic composition of the protolith to the granulites. Therefore this plot may be pointing to the derivation of felsic granulites by nearly closed-system metamorphism of pre-existing acid (granitic/rhyolitic) igneous rocks (Fiala et al. 1987a, b; Vellmer 1992; Janoušek et al. 2004) rather than by Variscan high-pressure partial melting (cf. Jakeš 1997; Kotková and Harley 1999). As assumed by Roberts and Finger (1997) and confirmed by thermodynamic modelling of Janoušek et al. (2004), there were probably present only limited amounts of melt (*c.* 10 vol. %) during any combination of the presumed peak conditions and the proposed granulite decompression paths.

Indeed, the felsic granulites show mostly undepleted LILE contents, arguing stoutly against their restitic nature. With the exception of the most mobile elements U, Th, Cs (± in some samples Rb), possibly stripped by a fluid or a small-scale melt (Fiala et al. 1987a, b; Vellmer 1992; Janoušek et al. 2004), their whole-rock geochemical signature was probably preserved regardless the HP–HT metamorphism they suffered. Much of the outstanding trace-element fingerprint (e.g. conspicuous depletions in Nb, Sr, Zr, Hf, and Ti) can be explained in the terms of the protolith composition and its development by K-feldspar, zircon and monazite fractionation (Janoušek et al. 2004).

Largely different seems to be the case of small bodies of the coeval syn-tectonic hyperpotassic granulites dealt with in the present contribution. They have been interpreted on the basis of the experimental work of Huang and Wyllie (1975; 1986) as dry, high-pressure (1.1–1.3 GPa and 850–950 °C) melts (Vrána 1989). In the Ab–Qz–Or ternary they plot close to the Or apex, in accord with the fact that during dry, high-pressure melting, it is the orthoclase that is the first phase to enter the non-eutectic melt (Vrána 1989; Schreyer 1999) (Fig. 13).

As argued above, the subducted (meta-) granitic crust was likely to yield, at HP–HT conditions, limited volumes of interstitial, K-rich melts. Their separation from the granulitic residue would be theoretically feasible as some authors suggested that even as little as 5 vol % of the granitic liquid can escape the source as soon as it forms interconnected network penetrating the whole rock volume (Brown 1994). This process would be even

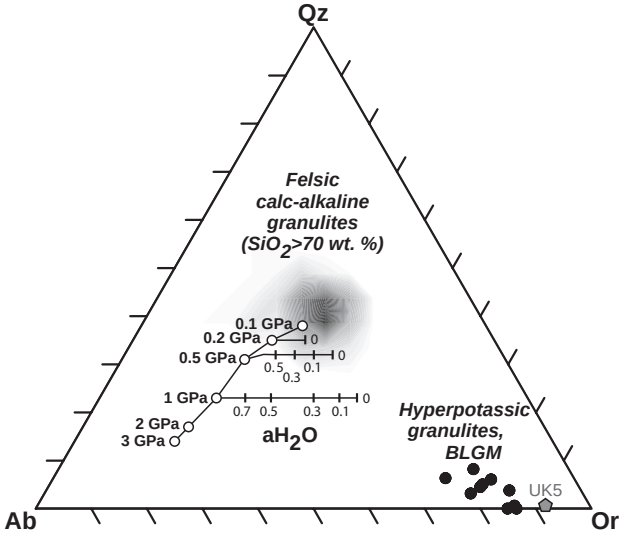

Fig. 13 The CIPW-normative Ab–Qz–Or ternary plot with frequency distribution of hyperpotassic granulites of the Blanský les Massif and felsic (SiO_2 > 70 wt. %) granulites from the whole Moldanubian Zone in Austria and Czech Republic (see Janoušek et al. 2004 for the data set and related references). Shown are also compositions of eutectics and minima in this system at various pressures as well as water activities (Johannes and Holtz 1996 and references therein). H_2O saturated melts: empty circles labelled by pressure in GPa (Johannes and Holtz 1996 and references therein); water-undersaturated melts at various water activities and pressures of 0.2, 0.5 and 1 GPa (Ebadi and Johannes 1991).

more efficient were the deformation involved (Rutter and Neumann 1995).

The low-volume melts produced would be most likely rich in incompatible trace elements such as U, Th, LREE and Zr (Finger and Cooke 2004). Figure 10c can be used for crude assessment of the balance for individual elements in course of the melting. The melt has been enriched, above all, in Zr and Hf; less so in LREE+MREE and Pb. However, in the hyperpotassic granulites the Th and Nb concentrations seem roughly comparable, and Ti much lower, than in the calc-alkaline lithologies (Fig. 10c). This may indicate that a Ti–Nb rich phase (rutile) has been left behind in the unmelted residue.

6.6. Fractional crystallization

Any model for development of hyperpotassic granulites needs to take into account microscopic observations, indicating the early growth of garnet/pyroxene and oscillatory-zoned (igneous) zircon, presence of large crystals of apatite (originally rather LREE rich), paucity of primary monazite together with relatively late crystallization of the K-feldspar matrix. The latter observation as well as the fact that the composition of the most felsic hyperpotassic granulites is close to that of K-feldspar, the most Si-rich primary phase in the rock, rules out fractionation driven by this phase. The whole-rock geochemical variation (increase in K, Na, Rb, Cs, Sr, Pb accompanied with sharp decrease in Fe, Mg, Zn, Sc, REE (in particular HREE), Y, Zr and P with increasing silica) argue stoutly for fractionation dominated by garnet, apatite and zircon. In theory the trends would be also compatible with unmixing of garnet-rich restite (Chappell et al. 1987; Litvinovsky et al. 2000); however the existence of euhedral zircon inclusions that have apparently nucleated at crystal faces of the garnet (Fig. 4f–g) seems to disprove it. In any case, the crystallization had to have been still at HT conditions, as demonstrated by the apatite and (some) zircon saturation temperatures exceeding 1000 °C.

The principal role for garnet in the fractionating assemblage is further supported by the R_1–R_2 diagram of De La Roche et al. (1980) modified by Batchelor and Bowden (1985) (Fig. 7d). Plotted are ideal mineral compositions of the main rock-forming minerals as well as fields for garnet (Grt) and zircon (Zrn) from the studied samples. Most of the hyperpotassic granulites form a roughly linear trend, developing towards progressively lower R_1 and R_2 values with rising silica, i.e. away from the garnet compositional field. The variation is consistent with a fractional crystallization controlled by this phase, with some contribution from zircon (Batchelor and Bowden 1985).

If true, most of the LILE (save Sr, incorporated, to some extent, into apatite) would be incompatible in the presumed crystallizing assemblage and thus would be passively enriched with progressing crystallization. The maximal possible degree of crystallization can be constrained using such strongly incompatible elements, as the Rayleigh Law

$$\frac{c_L}{c_0} = F^{(D-1)}$$

changes for D ~ 0 to:

$$\frac{c_L}{c_0} \approx \frac{1}{F}$$

where: c_L = concentration of a trace element in the fractionating melt, c_0 = initial concentration of this element in the (least fractionated) melt, F = fraction of the melt remaining.

The simple calculations using compositions of samples BD159 and LV122 (the least and most siliceous hyperpotassic granulites) would lead to maximal degrees of fractionation of 14 % (Rb), 35 % (Ba) and 38 % (K).

Even though some of these elements could have behaved slightly compatibly and/or may have been remobilized somewhat after the crystallization came to the end (Rb), this calculation shows the overall possibility of deriving the most felsic members of the suite by reasonable degrees (up to *c.* 40 %) of fractional crystallization.

6.7. Geotectonic model

As shown by Janoušek et al. (2004), the composition of felsic calc-alkaline granulites matches well that of orthogneisses and metarhyolites from the Fichtelgebirge, Saxothuringian Zone (Siebel et al. 1997; Wiegand 1997). This concerns whole-rock geochemistry (save Cs, Th and U that are much higher in the orthogneisses), Sr–Nd isotopic compositions as well as protolith ages falling within the spectrum of inherited ages observed in the granulites. Thus geochemically similar metaigneous crust produced during an Ordovician/Silurian rifting episode could have later yielded rocks resembling felsic calc-alkaline granulites upon subduction to depths of at least 50–60 km and temperatures > 1000 °C (O'Brien 2000; Janoušek and Holub 2007).

The HP–HT partial melting of the subducted metaigneous crust either at the metamorphic peak, or, more likely, in early stages of the uplift, could have produced limited volumes (< 10 %) of interstitial, *Or*-dominated melts rich in Zr, U, P and LREE. Some of these could have separated and accumulated to form small bodies similar to those observed in Plešovice, which further developed by HP–HT fractional crystallization of an assemblage dominated by garnet, apatite and zircon. On this basis it is considered likely that analogous occurrences will be discovered in other Moldanubian granulite bodies as well.

7. Conclusions

1. In the Blanský les granulite Massif, built mainly by felsic calc-alkaline, HP–HT garnet ± kyanite granulites, occur rare small bodies of garnet- (Plešovice type) or pyroxene-bearing (Lhotka type) hyperpotassic granulites.
2. The primary mineral assemblage of the Plešovice hyperpotassic granulites is dominated by perthitic K-feldspar and almandine–pyrope-rich garnet. The other conspicuously large euhedral crystals are apatite and zircon. Typical of the rock is also presence of rutile crystals, rich in Zr and Nb, as well as rare grains of primary monazite. The garnets are variously retrogressed (biotite ± secondary plagioclase, rutile and xenotime); from the primary apatite unmix small grains of Th-poor monazite.
3. The Lhotka type hyperpotassic granulites contain pyroxene (variously altered to actinolite) instead of garnet. The rock is dominated by perthitic K-feldspar, with a small amount of unmixed celsian. Typical are again large euhedral crystals of apatite with unmixed small grains of secondary monazite; primary monazite is rare. Noteworthy is the occurrence of secondary Ti phases with high contents of REE, Y and Zr, formed by decomposition of the primary pyroxene.
4. The studied granulites are highly potassic (K_2O > 7 %, up to *c.* 14 %, K_2O/Na_2O = 3.1–9.2 wt. %) and rather silica-poor (SiO_2 < 65 %) with comparably low contents most of major- and minor-element oxides, apart from potassium and phosphorus. Characteristic are high concentrations of Cs, Rb, Ba, U and K at variable enrichments in Zr and Hf. Whole-rock contents of some HFSE (Ti, Nb and Ta) are extremely low. The REE patterns show marked negative Eu anomalies and variable LREE enrichments increasing with rising silica due to a conspicuous drop in HREE.
5. The hyperpotassic granulites are interpreted as Viséan igneous rocks that crystallized, at relatively high-pressures, from hot (T > 1000 °C) magma with an unusual chemical composition. The Sr–Nd isotopic ratios document derivation from mature crustal sources (ε_{Nd}^{337} ~ -5.5; $^{87}Sr/^{86}Sr_{337}$ = 0.7272 and 0.7279 for the Plešovice and $^{87}Sr/^{86}Sr_{337}$ = 0.7109 for the Lhotka types). These data fall into the variation span of the normal calc-alkaline granulites but are substantially different from the typical Moldanubian metasediments.
6. Following the previous model (Vrána 1989), the genesis of the magma parental to the hyperpotassic granulites is explained by low degrees of HP–HT, non-eutectic partial melting. The low-scale melt was most likely expelled from calc-alkaline granulites common in the Moldanubian Unit as documented by analogous P-T conditions, similar age and complementary whole-rock geochemical and Sr–Nd isotopic signatures.
7. Subsequently the magma is thought to have developed by HP–HT fractional crystallization of an assemblage dominated by garnet, apatite and zircon, with or without some crystal accumulation.

Acknowledgements We are indebted to Petra Denková and Václav Kopecký for their assistance in the isotopic laboratory, as well as to Vojtěch Erban who measured the Sr–Nd isotopic ratios and provided helpful comments on an earlier version of the text. The short visit at Division of Earth Sciences, University of Glasgow (and patience of Colin Braithwaite in particular) made the acquisition of the CL photographs possible. A great part of this work originated during the research stay of VJ at the Institute of Mineralogy, University of Salzburg, in the framework of the FWF Project 15133–GEO. Further support from the Czech Grant Agency (GAČR 205/03/0040) is gratefully acknowledged.

This contribution benefited from thorough reviews of J. Sláma and an anonymous reviewer. It is dedicated to Stanislav Vrána, who described the occurrence of hyperpotassic granulites from the Blanský les Massif for the first time. He not only provided some of the samples and analyses presented in this paper, but it was him who introduced VJ to the dire straits of the granulite petrology and geochemistry.

References

Aftalion M, Bowes DR, Vrána S (1989) Early Carboniferous U–Pb zircon age of garnetiferous, perpotassic granulites, Blanský les massif, Czechoslovakia. Neu Jb Mineral, Mh 4: 145–152

Albarède F (1995) Introduction to Geochemical Modeling. Cambridge University Press, Cambridge, pp 1–543

Baker DR, Conte AM, Freda C, Ottolini L (2002) The effect of halogens on Zr diffusion and zircon dissolution in hydrous metaluminous granitic melts. Contrib Mineral Petrol 142: 666–678

Batchelor RA, Bowden P (1985) Petrogenetic interpretation of granitoid rock series using multicationic parameters. Chem Geol 48: 43–55

Becker H, Wenzel T, Volker F (1999) Geochemistry of glimmerite veins in peridotites from Lower Austria – implications for the origin of K-rich magmas in collision zones. J Petrol 40: 315–338

Benisek A, Finger F (1993) Factors controlling the development of prism faces in granite zircons: a microprobe study. Contrib Mineral Petrol 114: 441–451

Bingen B, Austrheim H, Whitehouse M (2001) Ilmenite as a source for zirconium during high-grade metamorphism?

Textural evidence from the Caledonides of Western Norway and implications for zircon geochronology. J Petrol 42: 355–375

Boynton WV (1984) Cosmochemistry of the rare earth elements: meteorite studies. In: Henderson P (ed) Rare Earth Element Geochemistry. Elsevier, Amsterdam, pp 63–114

Brown M (1994) The generation, segregation, ascent and emplacement of granite magma: the migmatite-to-crustally derived granite connection in thickened orogens. Earth Sci Rev 36: 83–130

Carswell DA, O'Brien PJ (1993) Thermobarometry and geotectonic significance of high-pressure granulites: examples from the Moldanubian zone of the Bohemian Massif in Lower Austria. J Petrol 34: 427–459

Chappell BW, White AJR, Wyborn D (1987) The importance of residual source material (restite) in granite petrogenesis. J Petrol 28: 571–604

Chen F, Hegner E, Todt W (1998) Garnet dating of granulites from the Variscan foldbelt in Central Europe; evidence for early and pre-Variscan high grade metamorphism. Acta Univ Carol, Geol 42: 221–222

Corfu F, Hanchar JM, Hoskin PWO, Kinny P (2003) Atlas of zircon textures. In: Hanchar JM, Hoskin PWO (eds) Zircon. Mineralogical Society of America and Geochemical Society Reviews in Mineralogy and Geochemistry 53, Washington, pp 469–503

Čadková Z, Jakeš P, Haková M, Mrázek P (1985) Geochemical catalogue of the basic network. MS of the Czech Geological Survey. In: Lithogeochemical Database of the Czech Geological Survey, Prague

Černý P, Novák M, Chapman R (1995) The Al (Nb, Ta) Ti_{-2} substitution in titanite: the emergence of a new species? Mineral Petrol 52: 61–73

Dallmeyer RD, Franke W, Weber K (eds) (1995) Pre-Permian Geology of Central and Eastern Europe. Springer, Berlin, pp 1–593

De La Roche H, Leterrier J, Grandclaude P, Marchal M (1980) A classification of volcanic and plutonic rocks using R1R2-diagram and major element analyses – its relationships with current nomenclature. Chem Geol 29: 183–210

Debon F, Le Fort P (1983) A chemical–mineralogical classification of common plutonic rocks and associations. Trans Roy Soc Edinb, Earth Sci 73: 135–149

Debon F, Le Fort P (1988) A cationic classification of common plutonic rocks and their magmatic associations: principles, method, applications. Bull Minéral 111: 493–510

Deer WA, Howie RA, Zussman J (1992) An Introduction to the Rock-Forming Minerals. Prentice Hall, pp 1–720

Degeling H, Eggins S, Elis DJ (2001) Zr budgets for metamorphic reactions, and the formation of zircon from garnet breakdown. Mineral Mag 65: 749–758

Dempster TJ, Jolivet M, Tubrett MN, Braithwaite CJR (2003) Magmatic zoning in apatite: a monitor of porosity and permeability change in granites. Contrib Mineral Petrol 145: 568–577

Donohue CL, Manning CE, Essene EJ (2001) The pressure and temperature dependence of Zr and Ti substitution in almandine. Geol Soc Am Abstr with Programs 33: 251

Ebadi A, Johannes W (1991) Beginning of melting and composition of first melts in the system Qz–Ab–Or–H_2O–CO_2. Contrib Mineral Petrol 106: 286–295

Esty WW, Banfield JD (2003) The Box-Percentile Plot. J Stat Software 8

Fediuková E (1978) Mafic minerals from granulites of the borehole Holubov (South Bohemian Moldanubicum). Sbor geol Věd, ložisk Geol Mineral 19: 169–198

Fiala J, Matějovská O, Vaňková V (1987a) Moldanubian granulites and related rocks: petrology, geochemistry, and radioactivity. Rozpr Čs Akad Věd, ř mat přír Věd 97: 1–102

Fiala J, Matějovská O, Vaňková V (1987b) Moldanubian granulites: source material and petrogenetic considerations. Neu Jb Mineral, Abh 157: 133–165

Fiala J, Fuchs G, Wendt JI (1995) Moldanubian Zone – Stratigraphy. In: Dallmeyer RD, Franke W, Weber K (eds) Pre-Permian Geology of Central and Eastern Europe. Springer, Berlin, pp 417–428

Finch AA, Klein J (1999) The causes and petrological significance of cathodoluminescence emissions from alkali feldspars. Contrib Mineral Petrol 135: 234–243

Finger F, Cooke R (2004) Evidence for the presence of trace-element-loaded interstitial partial melt in a Moldanubian leucocratic granulite derived from LA-ICP-MS analyses on zircons and rutiles In: Janoušek V (ed) International Workshop on Petrogenesis of Granulites and Related Rocks, Náměšť nad Oslavou, October 1–3, 2004. Excursion Guide & Abstract Volume. Moravian Museum, Brno, pp 35–36

Finger F, Krenn E (2007) Three metamorphic monazite generations in a high-pressure rock from the Bohemian Massif and the potentially important role of apatite in stimulating polyphase monazite growth along a PT loop. Lithos 95: 103–115

Finger F, Roberts MP, Haunschmid B, Schermaier A, Steyrer HP (1997) Variscan granitoids of central Europe: their typology, potential sources and tectonothermal relations. Mineral Petrol 61: 67–96

Finger F, Gerdes A, Janoušek V, René M, Riegler G (2007) Resolving the Variscan evolution of the Moldanubian sector of the Bohemian Massif: the significance of the Bavarian and the Moravo–Moldanubian tectonometamorphic phases. J Geosci 52: 9–28

Fleet ME, Pan Y (1995) Site preference of rare earth elements in fluorapatite. Amer Miner 80: 329–335

Fleet ME, Liu X, Pan Y (2000) Rare earth elements in chlorapatite [$Ca_{10}(PO_4)_6Cl_2$]: uptake, site preference and degradation of monoclinic structure. Amer Miner 85: 1437–1446

Foley SF, Venturelli G, Green DH, Toscani L (1987) Ultrapotassic rocks: characteristics, classification and constraints for petrogenetic models. Earth Sci Rev 24: 81–134

Forsythe LM, Nielsen RL, Fisk MR (1994) High-field-strength element partitioning between pyroxene and basaltic to dacitic magmas. Chem Geol 117: 107–125

Franěk J, Schulmann K, Lexa O (2006) Kinematic and rheological model of exhumation of high pressure granulites in the Variscan orogenic root: example of the Blanský les granulite, Bohemian Massif, Czech Republic. Mineral Petrol 86: 253–276

Franke W (1989) Tectonostratigraphic units in the Variscan belt of central Europe. In: Dallmeyer RD (ed) Terranes in Circum-Atlantic Paleozoic orogens. Geological Society of America Special Paper 230, pp 67–90

Franke W (2000) The mid-European segment of the Variscides: tectonostratigraphic units, terrane boundaries and plate tectonic evolution. In: Franke W, Haak V, Oncken O, Tanner D (eds) Orogenic Processes: Quantification and Modelling in the Variscan Belt. Geol Soc London Spec Pub 179: pp 35–61

Fraser G, Ellis D, Eggins S (1997) Zirconium abundance in granulite-facies minerals, with implications for zircon geochronology in high-grade rocks. Geology 25: 607–610

Fuchs G (1976) Zur Entwicklung der Böhmischen Masse. Jb Geol B-A 119: 45–61

Fuchs G, Matura A (1976) Zur Geologie des Kristallins der südlichen Böhmischen Masse. Jb Geol B-A 119: 1–43

Gallahan WE, Nielsen RL (1992) The partitioning of Sc, Y, and the rare earth elements between high-Ca pyroxene and natural mafic to intermediate lavas at 1 atmosphere. Geochim Cosmochim Acta 56: 2387–2404

Geake JE, Walker G, Telfer DJ (1977) The cause and significance of luminescence in lunar plagioclase. Philos Trans Roy Soc London A285: 403–408

Gebauer D, Friedl G (1994) A 1.38 Ga protolith age for the Dobra orthogneiss (Moldanubian zone of the southern Bohemian Massif, NE-Austria): evidence from ion-microprobe (SHRIMP) dating of zircon. J Czech Geol Soc 39: 34–35

Gerdes A (1997) Geochemische und thermische Modelle zur Frage der spätorogenen Granitgenese am Beispiel des Südböhmischen Batholiths: Basaltisches Underplating oder Krustenstapelung? Unpublished PhD. thesis, Georg-August-Universität, Göttingen, pp 1–113

Götze J, Habermann D, Neuser R D, Richter DK (1999) High-resolution spectrometric analysis of rare earth elements-activated cathodoluminescence in feldspar minerals. Chem Geol 153: 81–91

Götze J, Krbetschek MR, Habermann D, Wolf D (2000) High-resolution cathodoluminescence studies of feldspar minerals. In: Pagel M, Barbin V, Blanc P, Ohnenstetter D (eds) Cathodoluminescence in Geosciences. Springer, Berlin, pp 245–270

Green TH, Pearson NJ (1986) Rare-earth element partitioning between sphene and coexisting silicate liquid at high pressure and temperature. Chem Geol 55: 105–119

Gürtlerová P, Dušek P, Fikr Š (1997) Lithogeochemical database of the Czech Geological Survey. Czech Geological Survey Report 10167, Prague

Hack P J, Nielsen RL, Johnston AD (1994) Experimentally determined rare-earth element and Y partitioning behavior between clinopyroxene and basaltic liquids at pressures up to 20 kbar. Chem Geol 117: 89–105

Hanchar JM, Miller CF (1993) Zircon zonation patterns as revealed by cathodoluminescence and backscattered electron images: implications for interpretation of complex crustal histories. Chem Geol 110: 1–13

Harrison TM, Watson EB (1983) Kinetics of zircon dissolution and zirconium diffusion in granitic melts of variable water content. Contrib Mineral Petrol 84: 66–72

Harrison TM, Watson EB (1984) The behavior of apatite during crustal anatexis: equilibrium and kinetic considerations. Geochim Cosmochim Acta 48: 1467–1477

Holub FV, Janoušek V (2003) Geochemical and Sr–Nd isotopic constraints on the genesis of ultrapotassic plutonic rocks from the Moldanubian Zone of the Bohemian Massif. J Czech Geol Soc 48: 61–62

Huang WL, Wyllie PJ (1975) Melting reactions in the system $NaAlSi_3O_8$–$KAlSi_3O_8$–SiO_2 to 35 kilobars, dry and with excess water. J Geol 83: 737–748

Huang WL, Wyllie PJ (1986) Phase relationships of gabbro–tonalite–granite–water at 15 kbar with applications to differentiation and anatexis. Amer Miner 71: 301–316

Hutchison CS (1974) Laboratory Handbook of Petrographic Techniques. John Wiley & Sons, New York, pp 1–527

Icenhower J, London D (1996) Experimental partitioning of Rb, Cs, Sr, and Ba between alkali feldspar and peraluminous melt. Amer Miner 81: 719–734

Jacobsen SB, Wasserburg GJ (1980) Sm–Nd evolution of chondrites. Earth Planet Sci Lett 50: 139–155

Jakeš P (1997) Melting in high-P region – case of Bohemian granulites. Acta Univ Carol, Geol 41: 113–125

Janoušek V (2006) Saturnin, R language script for application of accessory-mineral saturation models in igneous geochemistry. Geol Carpathica 57: 131–142

Janoušek V, Holub FV (2007) The causal link between HP–HT metamorphism and ultrapotassic magmatism in collisional orogens: case study from the Moldanubian Zone of the Bohemian Massif. Proc Geol Assoc 118: 75–86

Janoušek V, Rogers G, Bowes DR (1995) Sr–Nd isotopic constraints on the petrogenesis of the Central Bohemian Pluton, Czech Republic. Geol Rundsch 84: 520–534

Janoušek V, Frýda J, Vokurka K (1996) Polyphase development of the Moldanubian granulites: evidence from the Rb–Sr and Sm–Nd isotopic study of the Blanský les granulite Massif (Czech Republic). In: Treloar P, O'Brien PJ (eds) What Drives Metamorphism and Metamorphic Reactions: Heat Production, Heat Transfer, Deformation and Kinetics? Kingston University, Kingston upon Thames, pp 43–44

Janoušek V, Vrána S, Erban V (2002) Petrology, geochemical character and petrogenesis of a Variscan postorogenic granite: case study from the Ševětín Massif, Moldanubian Batholith, Southern Bohemia. J Czech Geol Soc 47: 1–22

Janoušek V, Finger F, Roberts MP, Frýda J, Pin C, Dolejš D (2004) Deciphering petrogenesis of deeply buried granites: whole-rock geochemical constraints on the origin of largely undepleted felsic granulites from the Moldanubian Zone of the Bohemian Massif. Trans Roy Soc Edinb, Earth Sci 95: 141–159

Janoušek V, Farrow CM, Erban V (2006a) Interpretation of whole-rock geochemical data in igneous geochemistry: introducing Geochemical Data Toolkit (GCDkit). J Petrol 47: 1255–1259

Janoušek V, Gerdes A, Vrána S, Finger F, Erban V, Friedl G, Braithwaite CJR (2006b) Low-pressure granulites of the Lišov Massif, Southern Bohemia: Viséan metamorphism of Late Devonian plutonic arc rocks. J Petrol 47: 705–744

Janoušek V, Erban V, Farrow CM (2006c) Using the R language for graphical presentation and interpretation of compositional data in mineralogy: introducing the package GCDkit-Mineral. Austrian Association for Statistical Computing (AASC) and Wirtschaftsuniversität Wien, pp 84

Johannes W, Holtz F (1996) Petrogenesis and Experimental Petrology of Granitic Rocks. Springer, Berlin, pp 1–335

Johannsen A (1939) A Descriptive Petrography of Igneous Rocks I. University of Chicago Press, Chicago, pp 1–318

Kempe U, Götze J (2002) Cathodoluminescence (CL) behaviour and crystal chemistry of apatite from rare-metal deposits. Mineral Mag 66: 151–171

Kempe U, Gruner T, Nasdala L, Wolf D (2000) Relevance of cathodoluminescence for the interpretation of U–Pb zircon ages, with an example of an application to a study of zircons from the Saxonian Granulite Complex, Germany. In: Pagel M, Barbin V, Blanc P, Ohnenstetter D (eds) Cathodoluminescence in Geosciences. Springer, Berlin, pp 415–455

Keppler H (1993) Influence of fluorine on the enrichment of high field strength trace elements in granitic rocks. Contrib Mineral Petrol 114: 479–488

Kodym O (1972) Multiphase deformation in the Blanský les Granulite Massif. Krystalinikum 9: 91–105

Kodym O, Jakeš P, Schovánek P (1978) Granulite und ultramafische Gesteine aus der Strukturbohrung Holubov. Sbor geol Věd, Geol 32: 7–47

Kotková J (2007) High-pressure granulites of the Bohemian Massif: recent advances and open questions. J Geosci 52: 45–71

Kotková J, Harley SL (1999) Formation and evolution of high-pressure leucogranulites: experimental constraints and unresolved issues. Phys Chem Earth (A) 24: 299–304

Kröner A, O'Brien PJ, Nemchin AA, Pidgeon RT (2000) Zircon ages for high pressure granulites from South Bohemia, Czech Republic, and their connection to Carboniferous high temperature processes. Contrib Mineral Petrol 138: 127–142

Le Maitre RW (1982) Numerical Petrology. Elsevier, Amsterdam, pp 1–281

Leake BE, Wooley AR, Arps CES, Birch WD, Gilbert MC, Grice JD, Hawthorne FC, Kato A, Kisch HJ, Krivovichev VG, Linthout K, Laird J, Mandarino J, Maresch WV, Nickel EH, Rock NMS, Schumacher JC, Smith JC, Stephenson NCN, Whittaker EJW, Youzhi G (1997) Nomenclature of amphiboles: report of the Subcommittee on Amphiboles of the International Mineralogical Association Commission on New Minerals and Mineral Names. Mineral Mag 61: 295–321

Liew T C, Hofmann AW (1988) Precambrian crustal components, plutonic associations, plate environment of the Hercynian Fold Belt of Central Europe: indications from a Nd and Sr isotopic study. Contrib Mineral Petrol 98: 129–138

Liew TC, Finger F, Höck V (1989) The Moldanubian granitoid plutons in Austria: chemical and isotopic studies bearing on their environmental setting. Chem Geol 76: 41–55

Litvinovsky BA, Steele IM, Wickham SM (2000) Silicic magma formation in overthickened crust: melting of charnockite and leucogranite at 15, 20 and 25 kbar. J Petrol 41: 717–737

Lugmair GW, Marti K (1978) Lunar initial $^{143}Nd/^{144}Nd$: differential evolution line of the lunar crust and mantle. Earth Planet Sci Lett 39: 349–357

Marshall DJ (1988) Cathodoluminescence of Geological Materials. Unwin Hyman, Boston, pp 1–145

Matte P, Maluski H, Rajlich P, Franke W (1990) Terrane boundaries in the Bohemian Massif: result of large-scale Variscan shearing. Tectonophysics 177: 151–170

Medaris Jr. LG, Wang H, Jelínek E, Mihaljevič M, Jakeš P (2005) Characteristics and origins of diverse Variscan

peridotites in the Gföhl Nappe, Bohemian Massif, Czech Republic. Lithos 82: 1–23

Medaris Jr. LG, Beard B L, Jelínek E (2006) Mantle-derived, UHP garnet pyroxenite and eclogite in the Moldanubian Gföhl nappe, Bohemian Massif: a geochemical review, new P-T determinations, and tectonic interpretation. Int Geol Review 48: 765–777

Mitchell RH, Bergman SC (1991) Petrology of Lamproites. Springer, Berlin, pp 1–440

Mitchell RH, Xiong J, Mariano AN, Fleet ME (1997) Rare-earth element-activated cathodoluminescence in apatite. Canad Mineral 35: 979–998

Montel JM (1993) A model for monazite/melt equilibrium and application to the generation of granitic magmas. Chem Geol 110: 127–146

Morimoto N (1988) Nomenclature of pyroxenes. Mineral Mag 52: 535–550

Nasdala L, Zhang M, Kempe U, Panczer G, Gaft M, Andrut M, Plötze M (2003) Spectroscopic methods applied to zircon. In: Hanchar JM, Hoskin PWO (eds) Zircon. Mineralogical Society of America and Geochemical Society Reviews in Mineralogy and Geochemistry 53, Washington, pp 427–467

O'Brien PJ (2000) The fundamental Variscan problem: high-temperature metamorphism at different depths and high-pressure metamorphism at different temperatures. In: Franke W, Haak V, Oncken O, Tanner D (eds) Orogenic Processes: Quantification and Modelling in the Variscan Belt. Geol Soc London Spec Pub 179: pp 369–386

O'Brien PJ (2006) Type-locality granulites: high-pressure rocks formed at eclogite-facies conditions. Mineral Petrol 86: 161–175

O'Brien PJ, Carswell DA (1993) Tectonometamorphic evolution of the Bohemian Massif: evidence from high pressure metamorphic rocks. Geol Rundsch 82: 531–555

O'Brien PJ, Rötzler J (2003) High-pressure granulites: formation, recovery of peak conditions and implications for tectonics. J Metamorph Geol 21: 3–20

Owen JV, Dostal J (1996) Contrasting corona structures in mafic granulite from the Blanský Les complex, Bohemian Massif, Czech Republic. Canad Mineral 34: 959–966

Pin C, Vielzeuf D (1983) Granulites and related rocks in Variscan Median Europe: a dualistic interpretation. Tectonophysics 93: 47–74

Pin C, Zalduegui JFS (1997) Sequential separation of light rare-earth elements, thorium and uranium by miniaturized extraction chromatography: application to isotopic analyses of silicate rocks. Anal Chim Acta 339: 79–89

Pin C, Briot D, Bassin C, Poitrasson F (1994) Concomitant separation of strontium and samarium–neodymium for isotopic analysis in silicate samples, based on specific extraction chromatography. Anal Chim Acta 298: 209–217

Podor R, Cuney M (1997) Experimental study of Th-bearing $LaPO_4$ (780 °C, 200 MPa): Implications for monazite and actinide orthophosphate stability. Amer Miner 82: 765–771

Pupin J P (1980) Zircon and granite petrology. Contrib Mineral Petrol 73: 207–220

Racek M, Štípská P, Pitra P, Schulmann K, Lexa O (2006) Metamorphic record of burial and exhumation of orogenic lower and middle crust: a new tectonothermal model for the Drosendorf window (Bohemian Massif, Austria). Mineral Petrol 86: 221–251

Rajlich P, Synek J, Šarbach M, Schulmann K (1986) Hercynian-thrust related shear zones and deformation of the Varied Group on the contact of granulites (southern Moldanubian, Bohemian Massif). Geol Rundsch 75: 665–683

Rapp RP, Watson EB (1986) Monazite solubility and dissolution kinetics; implications for the thorium and light rare earth chemistry of felsic magmas. Contrib Mineral Petrol 94: 304–316

Roberts MP, Finger F (1997) Do U-Pb zircon ages from granulites reflect peak metamorphic conditions? Geology 25: 319–322

Roeder PL, Macarthur D, Ma XP, Palmer GR, Mariano AN (1987) Cathodoluminescence and microprobe study of rare-earth elements in apatite. Amer Miner 72: 801–811

Romer RL, Rötzler J (2001) P-T-t evolution of ultra-high-temperature granulites from the Saxon Granulite Massif, Germany. Part II: Geochronology. J Petrol 42: 2015–2032

Rønsbo JG (1989) Coupled substitutions involving REEs and Na and Si in apatites in alkaline rocks from the Ilimaussaq intrusion, South-Greenland, and the petrological implications. Amer Miner 74: 896–901

Rubatto D (2002) Zircon trace element geochemistry: partitioning with garnet and the link between U–Pb ages and metamorphism. Chem Geol 184: 123–138

Russell JK, Groat LA, Halleran AAD (1994) LREE-rich niobian titanite from Mount Bisson, British-Columbia – chemistry and exchange mechanisms. Canad Mineral 32: 575–587

Rutter EH, Neumann DHK (1995) Experimental deformation of partially molten Westerly Granite under fluid-absent conditions, with implications for the extraction of granitic magmas. J Geophys Res B100: 15697–15715

Schreyer W (1999) Experimental aspects of UHP metamorphism: granitic systems. Int Geol Review 41: 701–710

Schulmann K, Kröner A, Hegner E, Wendt I, Konopásek J, Lexa O, Štípská P (2005) Chronological constraints on the pre-orogenic history, burial and exhumation of deep-seated rocks along the eastern margin of the Variscan Orogen, Bohemian Massif, Czech Republic. Amer J Sci 305: 407–448

Siebel W, Raschka H, Irber W, Kreuzer H, Lenz KL, Höhndorf A, Wendt I (1997) Early Palaeozoic acid magmatism in the Saxothuringian belt: new insights from a geochemical and isotopic study of orthogneisses and metavolcanic rocks from the Fichtelgebirge, SE Germany. J Petrol 38: 203–230

Slabý J (1983) Modalní složení a petrochemie granulitů lišovského masívu a masívu Blanského lesa v jižních Čechách. Čas Mineral Geol 28: 41–60

Sláma J, Košler J, Schaltegger U, Tubrett M, Gutjahr M (2006) New natural zircon standard for laser ablation ICP MS U–Pb geochronology. In Winter Conference on Plasma Spectrochemistry, Tucson, Arizona, 8.–14. 1. 2006. ICP Information Newsletter 31: 187–188

Smith JV, Brown WL (1988) Feldspar Minerals 1. Crystal Structures, Physical, Chemical and Microtextural Properties. Springer, Berlin, pp 1–828

Sokol A, Domečka K, Breiter K, Janoušek V (2000) The underground storage near Příbram – a source of new information about granitoids of the Central Bohemian Pluton. Bull Czech Geol Surv 75: 89–104

Steiger RH, Jäger E (1977) Subcommission on Geochronology; convention on the use of decay constants in geo- and cosmochronology. Earth Planet Sci Lett 36: 359–362

Streckeisen A (1974) Classification and nomenclature of plutonic rocks. Geol Rundsch 63: 773–786

Strejček M (1986) Petrology of granulites in the Plešovice quarry near Český Krumlov. Unpublished MSci. Thesis, Charles University, Prague (in Czech)

Svojtka M, Košler J, Venera Z (2002) Dating granulite-facies structures and the exhumation of lower crust in the Moldanubian Zone of the Bohemian Massif. Int J Earth Sci (Geol Rundsch) 91: 373–385

Štípská P, Powell R (2005) Does ternary feldspar constrain the metamorphic conditions of high-grade meta-igneous rocks? Evidence from orthopyroxene granulites, Bohemian Massif. J Metamorph Geol 23: 627–647

Taylor SR, McLennan SM (1995) The geochemical evolution of the continental crust. Rev Geophys 33: 241–265

Tiepolo M, Oberti R, Vannucci R (2002) Trace-element incorporation in titanite: constraints from experimentally determined solid/liquid partition coefficients. Chem Geol 191: 105–119

Tollmann A (1982) Großräumiger variszischer Deckenbau im Moldanubikum und neue Gedanken zum Variszikum Europas. Geotektonische Forschungen 64, Stuttgart, pp 1–91

Tropper P, Konzett Y, Finger F (2005) Experimental constraints on the formation of high-P/high-T granulites in the Southern Bohemian Massif. Eur J Mineral 17: 343–356

Urban M (1992) Kinematics of the Variscan thrusting in the Eastern Moldanubicum (Bohemian Massif, Czechoslovakia): evidence from the Náměšť granulite massif. Tectonophysics 201: 371–391

Valbracht PJ, Vrána S, Beetsma JJ, Fiala J, Matějka D (1994) Sr and Nd isotopic determinations in three Moldanubian granulite massifs in southern Bohemia. J Czech Geol Soc 39: 114–114

van Breemen O, Aftalion M, Bowes DR, Dudek A, Mísař Z, Povondra P, Vrána S (1982) Geochronological studies of the Bohemian Massif, Czechoslovakia, and their significance in the evolution of Central Europe. Trans Roy Soc Edinb, Earth Sci 73: 89–108

Vellmer C (1992) Stoffbestand und Petrogenese von Granuliten und granitischen Gesteinen der südlichen Böhmischen Masse in Niederösterreich. Unpublished PhD. thesis, Georg-August-Universität, Göttingen, pp 1–111

Vellmer C, Wedepohl KH (1994) Geochemical characterization and origin of granitoids from the South Bohemian Batholith in Lower Austria. Contrib Mineral Petrol 118: 13–32

Villa IM (1998) Isotopic closure. Terra Nova 10: 42–47

Vrána S (1979) Polyphase shear folding and thrusting in the Moldanubicum of southern Bohemia. Věst Ústř úst geol 54: 75–86

Vrána S (1989) Perpotassic granulites from southern Bohemia: a new rock-type derived from partial melting of crustal rocks under upper mantle conditions. Contrib Mineral Petrol 103: 510–522

Vrána S (1992) The Moldanubian zone in Southern Bohemia: polyphase evolution of imbricated crustal and upper mantle segments. In: Kukal Z (ed) Proceedings of the 1st International Conference on the Bohemian Massif. Czech Geological Survey, Prague, pp 331–336

Vrána S (1998) Nový typ hyperdraselného granulitu v granulitovém masivu Blanského lesa. Zpr geol Výzk v Roce 1997, 52–53

Vrána S, Šrámek J (1999) Geological interpretation of detailed gravity survey of the granulite complex in southern Bohemia and its structure. Bull Czech Geol Surv 74: 261–277

Vuorinen JH, Hålenius U (2005) Nb-, Zr- and LREE-rich titanite from the Alnö alkaline complex: crystal chemistry and its importance as a petrogenetic indicator. Lithos 83: 128–142

Watson EB (1996) Dissolution, growth and survival of zircons during crustal fusion; kinetic principles, geological models and implications for isotopic inheritance. Trans Roy Soc Edinb, Earth Sci 87: 43–56

Watson EB, Harrison TM (1983) Zircon saturation revisited: temperature and composition effects in a variety of crustal magma types. Earth Planet Sci Lett 64: 295–304

Watson EB, Harrison TM (1984) Accessory minerals and the geochemical evolution of crustal magmatic systems: a summary and prospectus of experimental approaches. Phys Earth Planet Inter 35: 19–30

Waychunas G A (2002) Apatite luminescence. In: Kohn MJ, Rakovan J, Hughes JM (eds) Phosphates: Geochemical, Geobiological, and Materials Importance. Mineralogical Society of America Review in Mineralogy and Geochemistry 48, Washington, pp 701–742

Wendt JI, Kröner A, Fiala J, Todt W (1993) Evidence from zircon dating for existence of approximately 2.1 Ga old crystalline basement in southern Bohemia, Czech Republic. Geol Rundsch 82: 42–50

Wendt JI, Kröner A, Fiala J, Todt W (1994) U–Pb zircon and Sm–Nd dating of Moldanubian HP/HT granulites from south Bohemia, Czech Republic. J Geol Soc London 151: 83–90

Wiegand B (1997) Isotopengeologische und geochemische Untersuchungen zur prävariszischen magmatischen und sedimentären Entwicklung im saxothuringisch–moldanubischen Übergangsbereich (Grenzgebiet BRD/CR). Geotekt Forsch 88, Stuttgart, pp 1–177

Zack T, Moraes AR, Kronz A (2004) Temperature dependence of Zr in rutile: empirical calibration of a rutile thermometer. Contrib Mineral Petrol 148: 471–488

Zhang RY, Zhai SM, Fei YW, Liou JG (2003) Titanium solubility in coexisting garnet and clinopyroxene at very high pressure: the significance of exsolved rutile in garnet. Earth Planet Sci Lett 216: 591–601